Applications of THz spectroscopy in biosystems

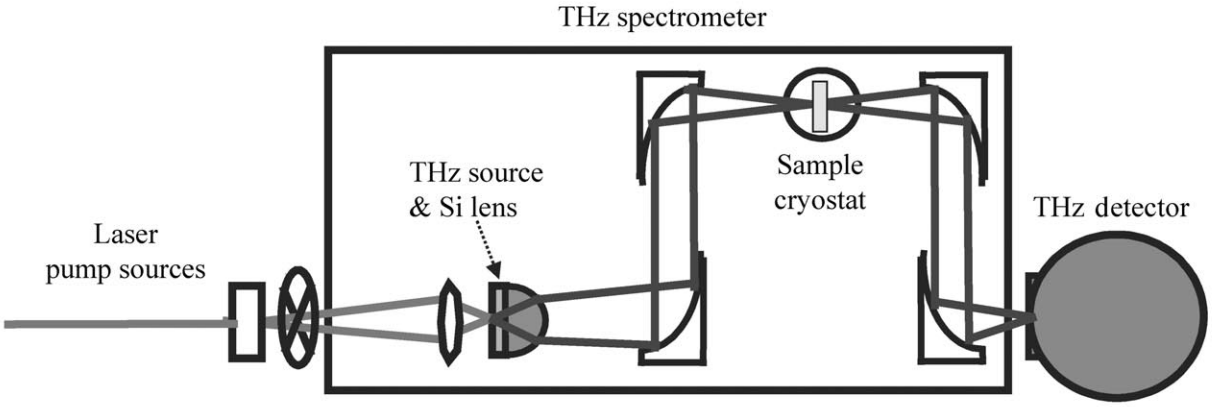

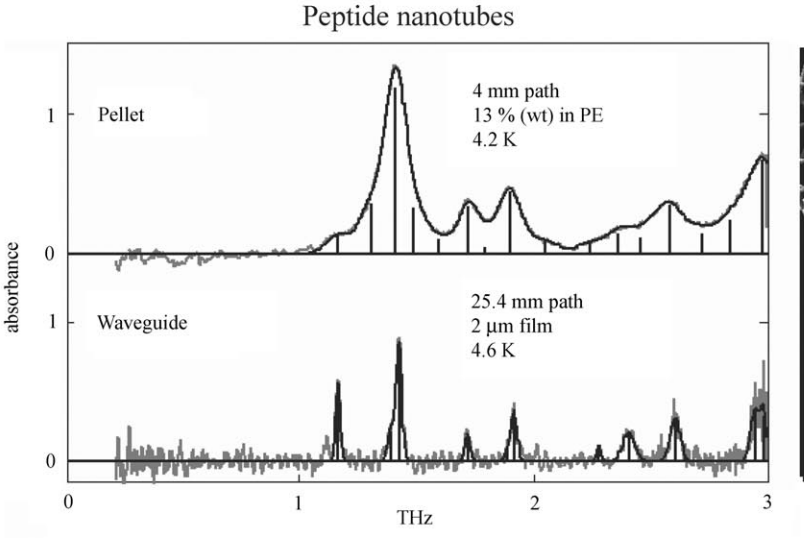

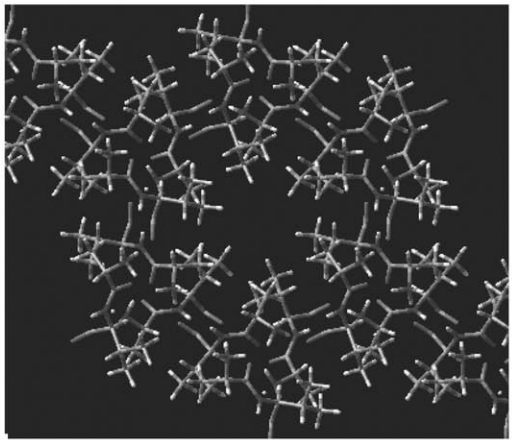

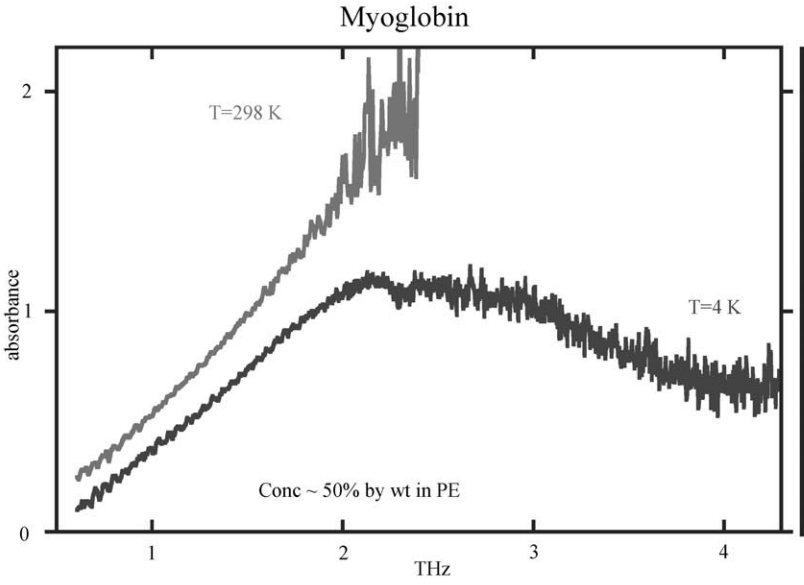

 DOI: 10.1002/cphc.200700332

DOI: 10.1002/cphc.200700332

Applications of Terahertz Spectroscopy in Biosystems

David F. Plusquellic,* Karen Siegrist, Edwin J. Heilweil, and Okan Esenturk[a]

Terahertz (THz) spectroscopic investigations of condensed-phase biological samples are reviewed ranging from the simple crystalline forms of amino acids, carbohydrates and polypeptides to the more complex aqueous forms of small proteins, DNA and RNA. Vibrationally resolved studies of crystalline samples have revealed the exquisite sensitivity of THz modes to crystalline order, temperature, conformational form, peptide sequence and local solvate environment and have given unprecedented measures of the binding force constants and anharmonic character of the force fields, properties necessary to improve predictability but not readily obtainable using any other method. These studies have provided benchmark vibrational data on extended periodic structures for direct comparisons with classical (CHARMm) and quantum chemical (density functional theory) theories. For the larger amorphous and/or aqueous phase samples, the THz modes form a continuum-like absorption that arises because of the full accessibility to conformational space and/or the rapid time scale for inter-conversion in these environments. Despite severe absorption by liquid water, detailed investigations have uncovered the photo- and hydration-induced conformational flexibility of proteins, the solvent shell depth of the water/biomolecule boundary layers and the solvent reorientation dynamics occurring in these interfacial layers that occur on sub-picosecond time scales. As such, THz spectroscopy has enhanced and extended the accessibility to intermolecular forces, length- and timescales important in biological structure and activity.

1. Introduction

In recent years, the terahertz (THz) spectral region from 0.06 THz (2 cm^{-1}) to 10 THz (333 cm^{-1}) has seen a flurry of research activity in the areas of biophysics and biochemistry. The resurgence is stimulated in large part by the rapid growth of new technologies needed to access this region and the unique sensitivity of this region to the global nuclear motions important in biomolecular processes. In particular, THz radiation is non-destructive and interrogates vibrational modes that extend across large portions of the biomolecular framework with length scales that extend over tens of angstroms. Such extended motions are important for the functioning of proteins/RNA/DNA that undergo transformations in secondary and tertiary structures.[1–7] A second advantage is realized in studies of biomolecular dynamics which span a range of timescales.[1–7] THz frequencies provide access to timescales in the sub-picosecond domain which are difficult to attain using other methods. Finally, the corresponding THz energy scale ranging from 0.04 kJ mol^{-1} to 4 kJ $mole^{-1}$ is a superset of the thermal energies required for biological activity and similar to the energies of dispersion (few kJ mol^{-1}) and hydrogen bonding (12 kJ mol^{-1}) that are responsible for this activity.

With the increasing awareness of these unique qualities, THz spectroscopy is emerging as an important tool to examine new aspects of biomolecular structure and dynamics. The collective, long-range nature of the nuclear motions and the "soft" force constants associated with the energy landscapes are strong functions of the conformational forms as well as the specific arrangement of intra and intermolecular hydrogen bonds. Consequently, when long-range order is retained as in crystalline solids, self-assembled layers, thin films, and so forth, this region contains the spectral fingerprints that correlate directly to three-dimensional structure and solvate environment. In the other extreme, large variations in the magnitudes of such interactions as present, for example, in amorphous samples or solutions can lead to severe inhomogeneous broadening and a "glass-like" absorption spectrum. While the resonant structure is largely hidden and masked by the severe absorption by liquid water,[8] the magnitude and frequency dependence of the THz response can provide insight into the global state of the system (native, denatured, single versus double-stranded helical form, etc.).

As the body of THz data grows in either limit, the greatest challenge to emerge is with the interpretation of results. Although high-resolution X-ray crystal structural data are of fundamental importance in biology, atomic coordinates by themselves give no direct information about the force fields. In contrast, optical techniques that gain access to THz vibrations such as Raman, low-energy neutron scattering[9] and direct absorption methods discussed here have exquisite sensitivity to these properties. As such, a key motivation for studies of biomolecular crystalline solids is to provide data to validate current force field models that are often used to improve our understanding of the structure and dynamics of much larger biosystems. While major advances in quantum chemical theory

[a] *Dr. D. F. Plusquellic, Dr. K. Siegrist, Dr. E. J. Heilweil, Dr. O. Esenturk*
Optical Technology Division
National Institute of Standards and Technology
Gaithersburg, MD 20899-8443 (USA)
Fax: (+1) 301-975-6991
E-mail: david.plusquellic@nist.gov

have been witnessed over the past few years, the challenge of achieving quantitative agreement with experiment at the classical level is immense and progress to date is still far from satisfactory. Nevertheless, the lack of agreement is itself illuminating and direct comparisons with quantum chemical theories can help pave the way forward for improved force field models as some of the studies discussed here will illustrate.

The focus of this review is on biomolecular applications of THz spectroscopy to studies ranging from crystalline solids including carbohydrates, polypeptides and other small biomole-

Edwin J. Heilweil received B.A. degrees in Chemistry and Mathematics and a M.A. degree in Physical Chemistry from Brandeis University in 1978. He went on to receive a Ph.D. in Physical Chemistry from the University of Pennsylvania in 1983. With advisor R. M. Hochstrasser, he developed time-resolved and nonlinear spectroscopic experiments to obtain ultrafast dynamical information for condensed-phase systems. From 1984–85, Dr. Heilweil held a NRC postdoctoral position at NIST and is currently a staff Research Chemist there. While at NIST, he received the Instrument Society of America Beckman award, Department of Commerce Stratton Award and the Sigma Xi Young Scientist award. He has authored over 80 technical papers, delivered 97 invited talks and holds one U.S. Patent. During 1986–1991, Dr. Heilweil applied picosecond and femtosecond laser methods to examine vibrational energy transfer and photochemical processes of molecules in gases, liquids and on solid surfaces. His current primary research interests include developing novel ultrafast infrared laser measurement methods, applying multiplexed infrared array detector techniques for chemical imaging and spectroscopy. Applications of THz technology are now being developed to monitor energy transfer and chemical reaction dynamics of biomolecular species in solution and in solids. Terahertz metrologies are also being extended to detecting threats and hidden objects in containers for Homeland Defense applications.

Karen M. Siegrist, born in 1960 in the USA, studied applied physics at the California Institute of Technology where she received her bachelor of science. She obtained a doctoral degree in physics at the University of Maryland with Ellen D. Williams in 2003, investigating surface field-induced and subsurface imaging mechanisms of the photoelectron emission microscope. She afterward came to the National Institute of Standards and Technology as a National Research Council postdoctoral fellow in the Physics Laboratory with Gerald Fraser and David Plusquellic and has continued at NIST as a guest researcher to the present. Her postdoctoral work has focused on high resolution THz spectroscopy of peptides and their interactions with solvents and the extension of THz spectroscopy to the study of thin films and layers.

David F. Plusquellic, born in 1960 in USA, studied physical chemistry at the University of Pittsburgh where he received his doctoral degree with David W. Pratt on the UV spectroscopy of hydrogen-bonded complexes of aromatic molecules. He went on to do postdoctoral work as an NRC fellow at JILA/University of Colorado with David J. Nesbitt investigating the unimolecular photodissociation dynamics of small molecules and clusters. In 1997, he joined the physics laboratory staff at the National Institute of Standards and Technology. He has authored over 50 technical papers, delivered 23 invited talks and holds one U.S. Patent. His work in the biophysics group focuses on the MW, THz and UV spectroscopy of small peptides and other biomolecules in the gas and condensed phases and the theoretical understanding of the biophysics of their interactions.

Okan Esenturk, born in 1972 in Turkey; received his BS and MS degrees in chemistry at METU (Turkey) and his PhD in physical chemistry from the University of Maryland (USA) under the guidance of Robert Walker. His doctoral study was on molecular structure effects at liquid/vapour interfaces using a self-made sum-frequency spectrometer. Okan is currently a postdoc at the NIST with Edwin Heilweil. He is investigating the application of THz spectroscopy on biologically small molecules and on photoconductive organic systems.

cules to thin films of partially hydrated and aqueous samples containing small proteins and DNA/RNA. Briefly discussed are three methods used in our labs for generating and detecting THz radiation which include 1) difference frequency mixing at the surface of a photoconductive switch (photomixer) using a continuous-wave source (THz-CWS), 2) difference frequency mixing in nonlinear optical media using a sub-picosecond light source (THz-TDS) and 3) a Fourier transform infrared spectrometer (FTIR) operating in the far-infrared (THz-FTIR). An overview is also given for the computational methods used to model some of the THz spectra presented in this review.

2. Experimental Procedures

Continuous-wave THz spectroscopy (THz-CWS) was used to measure spectra between 0.06–4.3 THz (3–125 cm^{-1}) at a resolution of $\approx$0.04 cm^{-1}. Details of this instrument have been given elsewhere.[10–12] Briefly, THz radiation was generated by the photomixing of two near-IR lasers at the surface of a low-temperature-grown GaAs photomixer.[13] The two lasers include a fixed-frequency diode laser operating near 850 nm ($\Delta\nu_{FWHM} \approx 0.0001$ cm^{-1}) and a standing-wave Ti:Sapphire (Ti:Sapp) laser having a resolution of $\Delta\nu_{FWHM} \approx 0.04$ cm^{-1}. The Ti:Sapp beam was combined with the output from a fixed frequency diode laser and focused by an aspherical lens onto the photomixer. For the spectra shown here, a maximum power of $\approx$1 μW of THz radiation was used although new ErAs:GaAs photomixers[14] are now generating ten times this power. The focused THz beam passes through the cryogenically cooled sample typically at 4.2 K and is detected by a liquid-helium-cooled silicon-composite bolometer. Power detection sensitivity of the bolometer is $<$1 nW up to 3 THz in a 400 Hz bandpass.

Lower-frequency THz time-domain spectroscopy (THz-TDS) was used to collect spectra between 0.4–8 THz (10–225 cm^{-1}) for solid disks and 0.4–2.7 THz (10–90 cm^{-1}) for liquid samples and compared to FTIR spectra whenever possible. The THz-TDS spectrometer we employ is now a common apparatus used in many of the studies discussed here and a review of the technique and setup are reported elsewhere.[15] Details and modifications made to our instrument to extend the typical 0.3–3 THz spectral bandwidth out to $\approx$8 THz have been given elsewhere.[16]

Infrared absorption spectra in the 0.2–22 THz range were obtained with a modified Nicolet Magna 550 Fourier transform infrared spectrometer (THz-FTIR) using a silicon-coated broadband beam-splitter and DTGS room-temperature detector fitted with a high-density polyethylene window. The FTIR with globar source has sufficient sensitivity to generate high-quality spectra in the 1.2–22 THz (40–700 cm^{-1}) range for both room-temperature pellets and samples placed in the liquid nitrogen or helium-cooled cryostat positioned in the sample compartment. All measurements were made after purging the sample compartment for $\approx$1 h to eliminate water vapor interference and after 64 interferometric averages at 4 cm^{-1} spectral resolution.

Spectra were converted to optical density (OD) units after ratioing raw sample transmission spectra (T_{sample}) to that of a pressed 100 mg polyethylene blank (T_{PE}) pellet ($OD = -\log_{10}[T_{sample}/T_{PE}]$) obtained under identical acquisition conditions. Absorption band intensities were also found to obey the Lambert–Beer law ($OD = \varepsilon cl$ where ε is the molar extinction coefficient, c the molar concentration and l the sample thickness) as the amount of sample is varied in several pellets of the same thickness and weight. This finding strongly indicates that all observed absorption features directly arise from the sample in the host matrix rather than from pellet mixing inhomogeneity or other optical anomalies.

Solid organic species (e.g. di-substituted benzenes) and lyophilized samples of individual purified amino acids and short polypeptides were used as received from Sigma–Aldrich, Inc. or ICN Biomedicals, Inc.[17] For all of the THz-CWS measurements, samples received from the manufacturer were first recrystallized from appropriate solvents using vapor diffusion methods. Most samples were stored at 273 K until use to prevent decomposition and exposure to atmospheric water. Matrix-diluted samples for THz absorption measurements were prepared by first weighing 2 to 10 mg of solid and homogenizing the material in a mortar and pestle to reduce the solid particle size distribution. This procedure ensures particle sizes sufficiently smaller than THz wavelengths to reduce baseline offsets at higher frequencies arising from non-resonant light scattering. Each sample was thoroughly mixed with approximately 100 mg of spectrophotometric grade high-density polyethylene powder (Sigma–Aldrich, Inc. with $<$150 μm particle size or MicroPowders, Inc.[17] with $<$10 μm particle size) and pressed as a $\approx$1 mm thick pellet in a 13 mm diameter vacuum die at the lowest possible pressures (ca. 200 psi or 1.4×10^6 Pa) to minimize decomposition from transient heating or high pressure.

To control temperature, the pellets were encapsulated in a brass fixture that adapts to the copper cold finger of a vacuum cryostat (Janis Research Company, Inc. model ST-100)[17] fitted with 3 mm thick high-density polyethylene windows for broadband infrared studies at 4, 10, 77 or 298 K.

3. Theoretical Spectral Modeling Methods

We give here an overview of the computational methods used to the predict minimum energy structures and THz vibrational spectra (at the harmonic level) presented in this review. As an essential task for the interpretation of THz data, these predictions provide insight into the nuclear motions that correlate to the observed absorption features. For the small crystalline (periodic) systems, results from quantum chemical methods have provided a means to evaluate the predictive quality of the classical force field model, CHARMm.[17] In some cases, such comparisons have been extended to small crystalline peptides containing the solvate, water. The latter results are particularly relevant since in the latter part of the review, CHARMm is used for the interpretation of experimental data obtained on larger biosystems in partially hydrated and aqueous environments. We note that other approaches for the classical calculation of lattice dynamics at THz frequencies have been reported by Day and co-workers[18] and alternative DFT codes that support

periodic boundary conditions include CRYSTAL,[19] VASP[20] and CASTEP.[21]

3.1 Gaussian 03 Calculations

To model the THz spectra of the non-hydrogen-bonded systems that include dicyanobenzene and dinitrobenzene, gas-phase DFT calculations were performed using the Gaussian software package (G03W Rev B.02)[22] with the Becke-3-Lee–Yang–Parr (B3LYP) functional and 6-311++G* basis set. Initial starting atomic geometries for each molecule were obtained from the NIST chemical structure database,[23] and the structures optimized as free space molecules. Positive (real) vibrational frequencies confirmed that minimum energy structures were obtained. Close agreement of bond lengths and angles with published crystallographic data provide some validation for the use of gas-phase models.

3.2 CHARMm Force Field Calculations

Calculations of the THz vibrational spectrum of the amino acids and polypeptides were accomplished using the CHARMm22 empirical force field.[24,25] In cases where water was present as a solvate, the TIP3P parameter set was used. The method used is similar to the previous work of Gregurick et al. for the calculation of the vibrational spectrum of small peptide[26] and sugar molecules.[27] In most cases, the crystallographically determined atomic coordinates were used as starting structures.[28–33] To model the crystal environment, periodic structures were created that consisted of a set of image cells surrounding the core block (typically one unit cell). The geometries were optimized using an adapted basis Newton–Raphson method until the gradient change was less than 10^{-4} kcal mol^{-1}. Using the steepest descent method, the structure was further optimized whereby all eigenvalues of the mass-weighted Hessian were positive (real). Convergence in the electrostatic energy sums was also ensured by using the Ewald approximation.[34,35] Finally, unit cells having the proper space group symmetry were confirmed by repeating calculations after increasing the core block size by two-fold or more along each crystallographic axis.

The THz vibrational frequencies were obtained from the normal mode eigenvalues of the mass-weighted Hessian and the intensities of each normal mode were calculated from the square of their dipole moment derivatives. The derivatives were calculated numerically from the atomic displacements along each normal mode. Computed spectra were represented by convoluting a Gaussian line shape function for each absorption peak using software such as that available in the package, JB95.[36]

3.3 DFT Calculations

DFT calculations were performed on the crystal structures of selected amino acids using the freeware program CPMD, version 3.9.2.[37] For L-serine, the calculation utilized the crystal structure coordinates[28–33] to define a unit cell containing four molecules and periodic boundary conditions to simulate the crystal lattice. The one-electron orbitals were expanded in a plane wave basis set with a kinetic energy cutoff of 80 Rydbergs restricted to the Gamma point of the Brillouin zone. Medium soft norm-conserving pseudo-potentials of Martins–Trouiller were used for all the elements.[38] The energy expectation values were computed in reciprocal space using the Kleinman–Bylander transformation.[39]

To calculate the intensities of each normal mode, we allowed the system to propagate for a total time of 5 ps by applying ab initio molecular dynamics using 600 a.u. for the fictitious mass of the electron. In these cases, a time step of 5 a.u. (0.12 fs) was used and positions and charges of each atom were recorded at every step. The total dipole moment was calculated at each step of the ab initio molecular dynamics using the Berry phase polarizability.[40] IR intensities were computed from the auto-correlation of the dipole magnitude followed by taking the Fourier transform.[41]

DFT calculations on the crystalline dipeptides and tripeptides were performed using the DMol^3 software package.[42] All calculations included all electrons and made use of a double numerical plus polarization (DNP) atomic orbital basis set (equivalent to a double-ζ). The exchange-correlation functional based on the generalized gradient approximation in the parametrization of Perdew and Wang (PW91)[43] was selected from among others tested for its predictive quality. The crystal cell parameters of the monoclinic cells were held fixed at the values reported from X-ray studies. The harmonic frequencies and normal mode displacements were calculated at the Gamma point by a two-point numerical differentiation of the forces. Similar to CHARMm, the intensity for each normal mode was calculated approximately from the Cartesian coordinate displacements and the static (Mulliken) atomic charges.

4. Small Biomolecules as Crystalline Solids

The THz spectra of biomolecular crystalline solids have been reported for a variety of oligopeptides, simple sugars, pharmaceutical species and other small biomolecules. In contrast to the larger systems discussed later, a common feature of these studies is the observation of a relatively small number of sharp vibrational features attributed to a discrete number of intramolecular and/or phonon modes of the solid. Observing vibrationally resolved features is primarily a result of two factors. Depending on the space group, typically only one or two conformations of the monomer subunits are dominant in the crystal and therefore, the small number of unique atoms per unit cell results in a small number of vibrational modes that are IR-active below 3 THz. Second, when employing the proper crystal growth procedures that minimize defects, narrow inhomogeneous linewidths (< 1 cm^{-1}) often result especially for systems where strong hydrogen-bonding networks exist throughout the solid. Moreover, at lower temperatures approaching 4 K, the spectral lines can significantly sharpen and shift depending on the impact of anharmonicity and crystal cage effects. Temperature-dependent studies can give information about the character of the mode as well as the anharmonicity

of the potential energy surface. A few examples that illustrate these properties will be presented below beginning with the experimental and theoretical results obtained for a non-biomolecular solid where hydrogen bonding interactions are absent.

4.1 Weakly Interacting Organic Compounds

In weakly associated solid-state systems, most intermolecular interactions are dominated by electrostatic and Van der Waals forces. Modeling these systems permits application of comparably fast DFT calculations using standard software packages (e.g. Gaussian 03) to identify internal and external vibrational modes of the solid systems rather than using of time-consuming solid state techniques. Calculated THz spectra of the 1,2-, 1,3- and 1,4-isomers of dicyanobenzene (DCB)[16] and related dinitrobenzene (DNOB) structures[44] which differ only by the ring location of the two cyano or nitro pendent side groups[45] are examples of such applications. Experimental and theoretical characteristics for the two benzene derivatives are briefly reviewed here.

Unlike mid-IR vibrational modes where the vibrations are typically localized within specific regions or pendent groups of the molecular structure, the vibrations of THz modes are global and involve motion of all atoms of the structure. Figure 1 shows a few examples of simulated THz modes for each isolated DNOB isomer along with their optimized structural parameters. Below 200 cm^{-1} (~6 THz), 1,2-DNOB has five IR-active modes while 1,3-DNOB exhibits only three modes. 1,4-DNOB has only two IR-active modes in this range due to inversion symmetry. However, both the calculated and experimental THz mode intensities increase by almost an order of magnitude as the NO groups are shifted from the 1,2- to the 1,4-positions (meta to para) of the benzene ring.

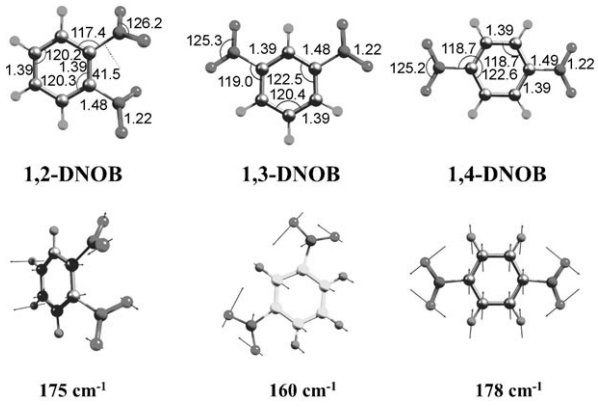

Figure 1. Dinitrobenzene structures and selected low frequency intramolecular modes shown as vibrational vector representations for the three species calculated with Gaussian 03W.

In Figure 2, we present the collection of experimental and theoretical vibrational spectra from gas-phase Gaussian 03 calculations, THz-FTIR for solutions (in $CHCl_3$) and solids (in PE matrix) measurements for all three isomers of DNOB at room temperature (ca. 298 K). As one can see, the calculated spectral frequencies and relative intensities closely match the experimental results, especially above 4 THz (~130 cm^{-1}). Comparing the measurements of solid to the liquid-phase samples (thus eliminating intermolecular mode absorptions) shows that these systems exhibit only one or two infrared-active intermolecular (phonon) features for all three species in the spectral region below 6 THz (between 40–200 cm^{-1}). Similar results were also observed and calculated for the DCB isomers.[16] As found here for DNOB, the DCB isomer study showed that the strongly coupled electro-negative cyano groups coordinated to the π-bonded benzene ring affords the possibility that partial atomic charges undergoing low frequency vibrational motions enhance the THz absorption intensities.

These studies yielded two significant observations: 1) The Gaussian 03 software package may be reliably used to interpret the low-frequency THz spectral region for weakly interacting organic systems and help to distinguish and classify the observed vibrational features as intramolecular or intermolecular (phonon) modes. These studies of dinitro- and dicyanobenzenes show that DFT with B3LYP/6-311G* or higher order basis sets predicts the solid-state equilibrium structure and internal modes with reasonably good accuracy for systems exhibiting

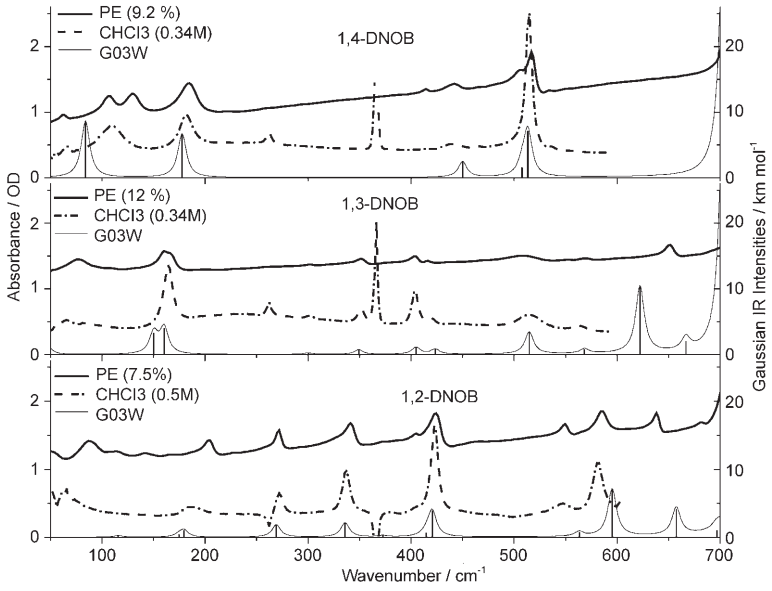

Figure 2. Experimental (THz-FTIR) and calculated spectra for three dinitrobenzene isomers at 298 K. Weight percent for PE solid pellets (——, top) and chloroform concentrations (-----, middle) are noted in each panel. A sharp interfering chloroform band occurs at 365 cm^{-1}.

only weak intermolecular interactions in the solid phase. 2) To our knowledge, the observed intensities of the lowest two phonon modes of 1,4-DCB are the strongest THz absorption features (per molecule) reported to date. The DCB isomers and their identifiable spectral features may be of interest in future studies utilizing THz spectroscopy to analyze the internal verses phonon modes of solids.[46]

4.2 Amino Acids

In an effort to reveal the underlying THz spectral contributions from the individual amino acids of a protein, we began a series of experiments to measure the THz-infrared absorption spectra for many of the twenty naturally occurring solid-state (lyophilized) amino acids. As discussed below, we found that these spectra contain a dense set of absorption features in the 1–22 THz (33–700 cm^{-1}) spectral range.[47]

We obtained the solid-state spectra for L-serine and L-cysteine to determine whether an atomic substitution (–OH for serine versus –SH for cysteine) can be identified in the THz spectrum.[48] Significant differences were noted, especially in the lower frequency phonon region ($< 100\ cm^{-1}$) indicating the crystalline lattice interactions are strongly affected by the simple atomic substitution. Rungaswang et al.[49] have recently reported on the anisotopic parameters of single crystals of L-cysteine and L-histidine using THz-TDS which contain information about the orientation of transition dipoles of the THz modes.

THz spectroscopy is also highly sensitive to the enantiomeric crystalline structure of biomolecules. The stereochemistry of many biological and pharmaceutical species plays a significant role in its functionality and toxicity. Investigations into the THz spectrum of enantiomeric mixtures and compounds of left and right-handed species have been reported by Yamaguchi et al.[50] and Fischer et al.[51] In our group,[52] spectra for L-, D-tryptophan (Trp) and the 1:1 mixture of DL-Trp as well as various mixtures were studied using THz-FTIR spectroscopy. While the spectra for pure D- and L-Try are identical, admixtures from approximately 5 mol% to 50 mol% could readily be identified from changes in absorption intensities of several spectral features in agreement with similar results reported by Yamaguchi et al.[50] Figure 3 shows examples of the Trp spectra as well as a single fluorine-substituted analog which generates a completely different spectrum compared to the native amino acid. Principle component spectral analysis is readily applicable to such data to quickly analyze and extract "contaminant" concentrations, a task which is difficult using other analytical methods.

Starting from available X-ray crystal structures for each amino acid species,[23] application of inexpensive gas-phase DFT methods[22] did not produce predicted THz spectra that agreed well with experiment. Apparently, the currently applied basis sets or parameterized potential energy functions are not adequate to model the intermolecular hydrogen bonding properties of these systems. Better agreement was found from periodic system calculations using CHARMm and CPMD as shown in our publication.[48]

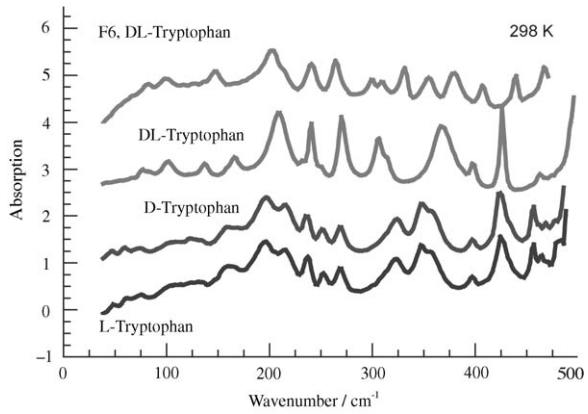

Figure 3. Experimental THz absorption spectra (THz-FTIR) for the pure D- and L-Tryptophan (Trp) enantiomers, their 1:1 mixture (DL-Trp) and F6-fluorine substituted DL-Trp amino acid in the solid state. Comparison of the L-Trp and D-Trp stereoisomers shows the spectra are identical, while the DL-Trp mixture has a distinctly different spectrum. The F6-DL-Trp species also shows different spectral features than the DL-Trp mixture.

4.3 Polypeptides

The series of di-peptides nanotubes, Ala-Val,[53] Ile-Ala,[54] Val-Val,[54] Ile-Val[54] plus their retro-analogs,[54,55] have been investigated in our group using THz-CWS methods.[56,57] The THz spectra obtained at 4.2 K in polyethylene pellets are shown in Figure 4. Also shown are the best-fit simulations to provide some assessment of the number of features in each spectrum. Each simulation consists of the sum of Gaussian functions that account for the absorption intensity. The X-ray crystallographic studies of these solids have revealed structures consisting of hydrophobic core regions lined with the side chain (R) groups with tube diameters that decrease with increasing side chain size from roughly 5.2 Å to 3.3 Å. Furthermore, some of the nanotubes studied here are large enough to support the solvate, water.[54] We have found that the THz spectra are rather insensitive to presence of water in the nanotubes. (This is in sharp contrast to the hydrated form of tri-alanine). The spectra of the hydrated forms (not shown) are overall very similar except for small 1–2 cm^{-1} spectral shifts and hence, the solvate interactions with the hydrophobic tubes are minimal.[56]

For all of these systems, the spectra features at 4.2 K are rather severely broadened with widths ranging between 2–3 cm^{-1}. To significantly reduce the width of these features, a quasi-optical waveguide technology pioneered by Grischkowsky[46,58–60] and co-workers has been recently developed in our labs. An example of preliminary data on the Val-Ala nanotube is shown at the bottom of Figure 5 together with the THz spectrum from the pellet shown above it. Although all the important features appear in both spectra, peaks in the thin film spectrum are as much as five-fold narrower than the same features found for the pellet sample. Similar observations have already been reported by Grischkowsky and co-workers[60] for deoxycytidine and D-glucose. For example, the strongest peak in the THz spectrum of Val-Ala appears at 47.1 cm^{-1} with a fitted Gaussian width of 4.2 cm^{-1} compared to a width of

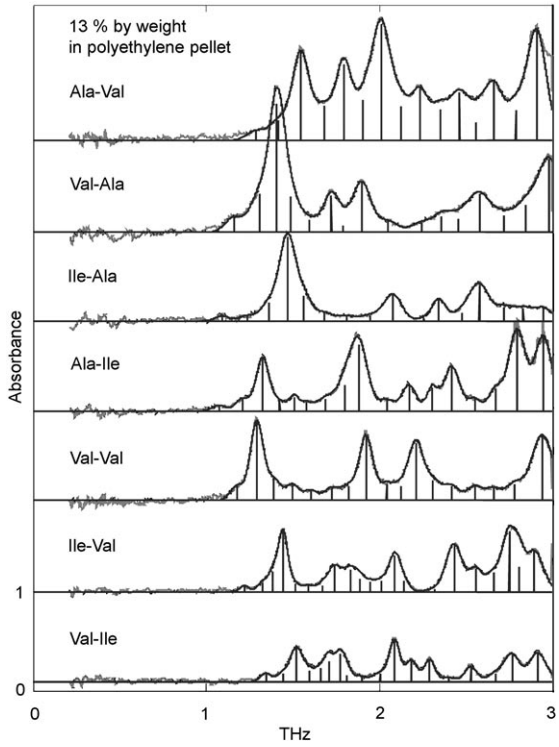

Figure 4. THz (THz-CWS) spectra at 4.2 K of a series of dipeptide nanotubes (P61 space group) having hydrophobic core regions consisting of different side chain groups. The best-fit simulated spectra are also shown superimposed. Each simulation consists of the sum of Gaussian functions centered on the sticks. The spectra have been normalized to sample concentration and pathlength and offset along the ordinate by 1 OD (base 10) absorbance unit for clarity. The top-to-bottom order is given in terms of decreasing core size and illustrates the general shift of spectral features to higher frequency as steric repulsion increases within the tubes.

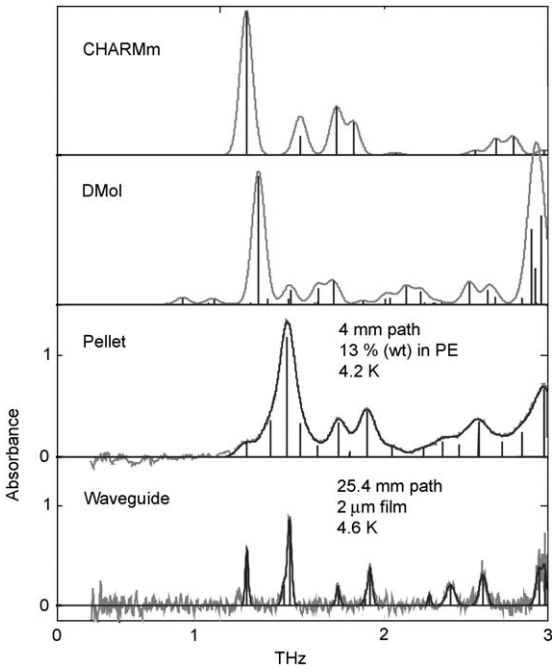

Figure 5. Comparison of the observed THz-CWS spectra of Val-Ala dipeptide nanotube observed in a waveguide (250 μm gap) as a thin film (Waveguide) and in a polyethylene pellet (Pellet). Approximately 1 mg remains of a sample dropcast on the waveguide surface 6 mm wide and 25.4 cm in (optical) depth giving a film of ≈2 μm thick. Pellet samples consisted of 11 mg of sample in PE in a 12.5 cm in diameter, 0.75 mm thick disk. Overlayed on the experimental traces are the best-fit simulated spectra consisting of a sum of Gaussian peaks centered on the sticks. Predictions are also shown from quantum chemical (DFT/PW91) and classical (CHARMm) theories.

0.75 cm^{-1} for the same feature at 47.4 cm^{-1} in the thin film spectrum. The other features are likewise narrowed by a similar factor. Notice also that some of the spectral intensities are different for the two samples. These results suggest that in-plane orientation of the Val-Ala crystals have a defined in-plane orientation relative to both the surface and the polarization supported by the waveguide.[60] Therefore, additional information regarding the types of nuclear motion associated with these absorption features may be obtained when this orientation is known.[60]

The simplicity of these systems (hexagonal space group symmetry) has permitted extensive theoretical studies at the classical and quantum levels. The spectral predictions from DFT/PW91 (DMol^3) are shown for Val-Ala in Figure 5. Although some improvement is still needed, the DFT results clearly reproduce many of the observed features. Spectral predictions of similar quality are found for the other members of the series.[57] The CHARMm results are also shown in Figure 5 and while the main features are predicted, some of the weaker lines are missing. Furthermore, the corresponding nuclear motions at the two levels of theory are very different. We are currently exploring whether the sources of the discrepancies arise from intramolecular factors or from the longer range dispersion and/or hydrogen bonding effects. For example, through comparisons with gas phase microwave results of peptide mimetics, we have found the size of isolated monomers in β-[61,62] and γ-[63] conformations are overestimated and conformational methyl group minima are sometimes opposite to those predicted by correlation-corrected theories.[64] Such errors are likely caused by an underestimation of dispersion interactions at the DFT level. Finally, current efforts are directed towards the determination of the crystal orientation relative to the waveguide surface to better correlate the nuclear motions with absorption features and provide further validation of these theories.[60]

The sensitivity of the THz region to different β-sheet structures and the impact of the solvate, water was investigated in our group using THz-CWS[65] for three different crystalline forms of the alanine tripeptide, NH_3^+–Ala_3–O^-. Depending on the conditions during recrystallization, trialanine is known from X-ray crystal studies[66] to exist in one of two β-sheet forms, a dehydrated parallel β-sheet (*p*-Ala_3) and a hydrated anti-parallel β-sheet (*ap*-Ala_3–H_2O). The latter form was also reported using THz-TDS methods at nearly the same time.[67] A third form discovered in this study was the dehydrated form, *ap*-Ala_3. As shown in Figure 6, the THz spectra (0.6–100 cm^{-1}) obtained at 4.2 K for the three forms are qualitatively different. This difference is in sharp contrast to the mid-IR region where the FTIR spectrum[68] of *ap*-Ala_3-H_2O is similar to that of the *p*-Ala_3 and nearly identical to the dehydrated form, *ap*-Ala_3.[65]

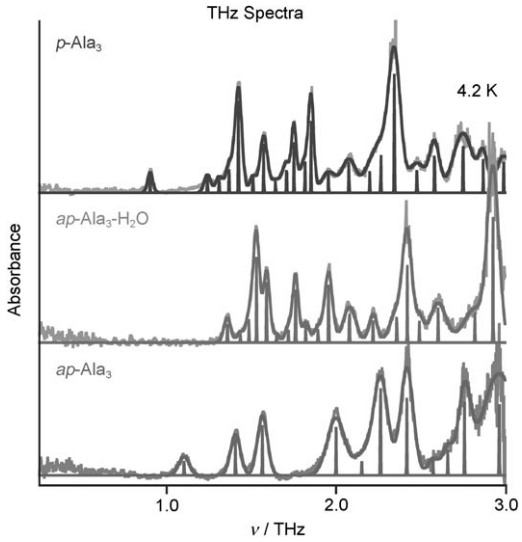

Figure 6. THz absorption spectra (THz-CWS) of the three different crystalline forms of trialanine. Overlayed on each spectrum are the best-fit simulated spectra that consist of the sum of Gaussian peaks centered on the sticks. While the conformational forms of the monomers are similar, the parallel (*p*) and hydrated anti-parallel (*ap*) β-sheets have different space group symmetries (P12 and C2, respectively—the dehydrated form is unknown but likely C2). These spectra indicate the enormous sensitivity to the β-sheet form and the hydrogen bonded (structurally bound) water.

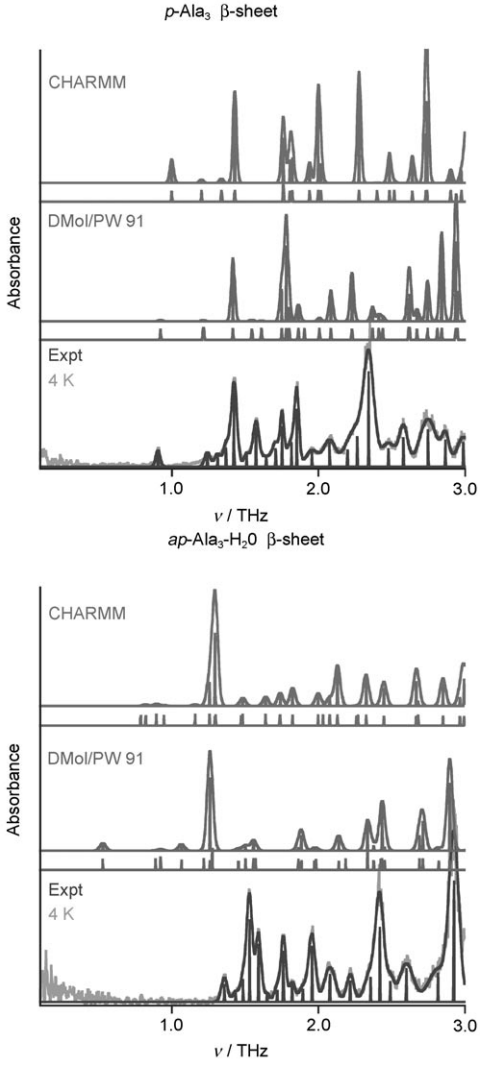

Figure 7. Predicted and observed THz spectra of the parallel (top) and hydrated anti-parallel (bottom) β-sheet forms of crystalline trialanine from DFT/PW91 (DMol^3 software suite) and CHARMm.

The significance of this result is the dramatic impact the solvate, water and the arrangement of hydrogen bonds have upon the THz spectrum, since the conformational forms of the monomers are known to be similar from structural parameters reported in the X-ray crystal studies.[66]

The small size of these systems enabled rigorous comparisons with quantum chemical (DFT) and classical models (CHARMm). In sharp contrast to the weakly bound organic systems discussed above, calculations on these hydrogen-bonded crystals required the use of periodic boundary conditions. Results from the DFT calculations using the DMol^3 program suite[42] are shown together with experiment in Figure 7 for the parallel and hydrated anti-parallel sheet forms. Spectral predictions of the parallel sheet with its highly cross-linked hydrogen bonding network are in fair agreement with many of the observed features. However, the treatment of the weaker inter-sheet binding in the anti-parallel sheets is a severe challenge for theory where clearly the current level fails to achieve qualitative agreement. Furthermore, a normal mode projection analysis of the CHARMm and DFT predictions in Figure 7 indicate that the similarities regarding spectral predictions were accidental since the corresponding nuclear motions at these two levels were vastly different.[65]

These results suggest the need for improved density functionals that target multi-body effects present in hydrogen bonding networks and improved force field models that include polarizability terms for water and three-atom hydrogen bonding terms for periodic solids. Current theoretical studies are underway 1) that use a triple zeta basis set and a fully relaxed crystalline cell geometry at the DFT level and 2) that treat anharmonicity of the modes using VSCF theory at the classical level.[69]

Because polypeptides have C- and N-terminations and are therefore sequence specific, we investigated a series of polypeptides using THz-FTIR to examine whether their crystalline forms yield qualitatively different THz spectra. As may be seen in Figure 8, every peptide that was examined, including reverse sequences produced a different and readily identifiable spectrum. From these results, it can be concluded that short-chain crystalline polypeptides may be uniquely "fingerprinted" by simply acquiring the THz spectrum in the 50–500 cm^{-1} spectral range. Several mixed polypeptide sequences with up to three amino acids were also studied (e.g. Val-Gly-Gly, glutathione) but sharp spectral features were not present for species containing more than ten amino acids. This observation may be the result of increasing spectral density as the molecular weight increases, or the spectral features are swamped by hydrogen-bonded water which is difficult to remove from these complex biomaterials.

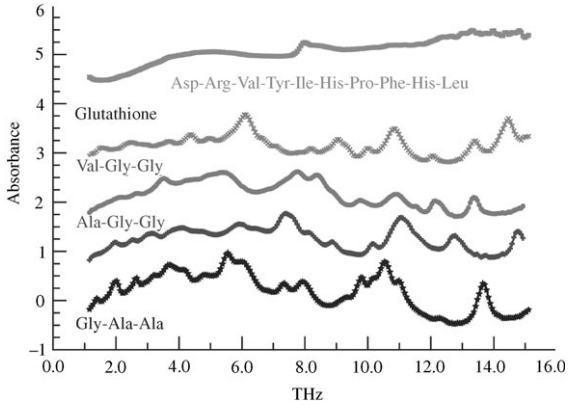

Figure 8. Representative THz infrared absorption spectra for several di- and tri-peptides showing the variability in spectral content and uniqueness for each structure. For comparison (top), a random sequence 10-mer is also shown and exhibits loss of distinguishing absorptions, most likely from spectral overlap or hydration.

4.4 Nucleic Acid Bases and Other Sugars

Fisher et al.[70] studied the dielectric function of the four nucleobases, adenine (A), guanine (G), cytosine (C) and thymine (T) and their corresponding nucleosides, dA, dG, dC and dT (d = deoxyribose) of DNA from 0.5–4.0 THz at 10 K and 300 K using THz-TDS. The spectra of A, G, C and T are dominated by absorption features between 1–3.5 THz. At 10 K, the broad room temperature features blue shift by 5% and resolve into several narrow peaks. The blue shift with decreasing temperature is attributed to decreasing bond lengths. The spectra of dA, dG, dC and dT above 1.5 THz are similar to the nucleobases but a second group of resonances from 1–2 THz have narrow asymmetric line shapes attributed to the sugar groups.

Quantum chemical calculation were performed on the gas-phase tetramer of thymine using density functional theory (B3LYP/6-31G basis). The absorption spectrum and index of refraction were calculated for the minimum energy geometry (beginning with the X-ray crystal structure) and compared with experiment. The calculations predict four low frequency IR-active modes arising from in-plane and out-of-plane intermolecular motions of the hydrogen bonded cluster. Although definitive assignments were not possible, the correct number of features was reproduced nevertheless. More recent calculations[71] on the pentamer single-stranded sequence (ATATA) were shown to be in very good agreement with experiment while similar comparisons on higher oligomers (for example, the octomer) were not as satisfactory. The observation of the well-resolved and distinct spectral fingerprints of the nucleobases and nucleosides arising from the arrangement of the molecules in the microcrystalline structures is noteworthy.

Grischkowsky and co-workers have applied THz-TDS to thin film (pure) samples of deoxycytidine and D-glucose[60] prepared in a single mode waveguide to enhance detection sensitivity, improve the spectral resolution (up to five fold) and polarization resolve oriented crystals at the surface.[46,58,59] A THz pulse was coupled through a 50-micron-gap plane-parallel waveguide using a pair of silicon cylindrical lenses. Confinement of the THz electric field in the waveguide resulted in a stronger interaction with the thin film sample than possible in pellet samples leading to a sensitivity enhancement proportional to the ratio of waveguide length to plate separation.

From the results of thin films of deoxycytidine at 77 K,[60] at least seven lines were observed between 1.5–3 THz with linewidths (FWHM) on the order of 1 cm^{-1} or less. These widths were much narrower than results from pellet studies at 10 K discussed below.[72] Glucose also showed significant line narrowing compared to results from pellet samples.[73] The high degree of crystalline order on the waveguide compared to randomly oriented crystals in the pellet are believed to account for the reduction in the inhomogeneous linewidth.

Shen and co-workers have used THz-TDS (0.2–3 THz) to obtain THz spectra of the nucleic acid bases adenine and purine[74] and the four nucleosides, adenosine, thymidine, cytidine, and guanosine[72] in pressed disks of powder samples (10% by weight in polyethylene) over the temperature range from 4–290 K. For these samples, spectra that were mostly unresolved at 290 K showed several sharp, well-defined features at 4 K. A study of the purine sample revealed that most of the five sharp features observed at 4 K shifted to lower frequency and broadened above 50 K. For adenosine, thymidine, cytidine, and guanosine, the sharp spectral features identified at 4 K were also shown to broaden and red-shift with increasing temperature. In all cases, the frequency shifts with temperature were fit to a Bose–Einstein distribution model parameterized by a frequency υ_0, a critical mode temperature T_C and a constant A. The authors suggested that the anharmonic components of the potentials may also contribute to the temperature-dependent behavior of these samples. In the latter study, it is demonstrated that THz-TDS can be used to distinguish the positions of the different nucleosides placed at a separation of 1.5 mm in a four-slot holder as it is moved across the THz focus.

Shen and et al.[75] also performed time-resolved studies of cytosine prepared in polyethylene using THz-TDS. Transmission spectra of the cytosine sample showed an absorption dip at 1.7 THz for the initial 3 ps but at longer times (7–12 ps), the transmission spectrum revealed an emission peak at 1.7 THz. For intermediate times of 3–6 ps, an intermediate state was observed, the lifetime of which was estimated at 6.5 ps from fitting to the expression for the decaying field emitted by a radiating molecule.

The THz dielectric properties of the three sugars, glucose, fructose and (protonated and deuterated) sucrose were studied by the Walther et al.[73] from 0.5–4.0 THz using THz-TDS. Crystalline forms were shown to have sharp features while absorption by the amorphous forms was featureless and increased monotonically with frequency. With increasing temperature, all absorption features of glucose and fructose broadened and red-shifted. However, for sucrose, the two lowest frequency resonances of the protonated and deuterated samples (peak 1 at 1.38/1.28 THz for the protonated/deuterated forms and peak 2 at 1.69/1.63 THz) initially blue shifted with increasing temperature and then above a crossover temperature

(240 K for peak 1 and 120 K for peak 2), shifted to lower energy. They found the frequency shifts with deuteration $\Delta\nu/\nu = -7\%$ and -3.5% are larger than expected based on simple harmonic mass weighting alone ($\Delta\nu/\nu \sim 1.2\%$). Furthermore, they argue the anomalous blue shift is not easily explained based on vibrational anharmonicity since red-shifts arising from hydrogen bonding stretch potentials are expected with increasing temperature. They suggest the initial blue shift at low temperatures may be a result of the relatively larger impact of van der Waals forces on the hydrogen bonding potentials compared to the higher temperature limit where anharmonicity presumably dominates. Recently, Unterrainer and co-workers[76] have reported the anisotropic optical parameters of single crystals of sucrose at 5 K using THz-TDS which contain important information about the orientation of transition dipoles of the THz modes.

Temperature-dependent THz spectra (0.1–3.0 THz) of the monosaccharides, D-glucose, D-mannose, D-galactose, and D-fructose and the disaccharides, maltose and lactose were examined by Shen and co-workers[77] in polyethylene pellets using THz-TDS. At 4 K, all four monosaccharides showed unique spectra with several well-defined features, most falling above 1.5 THz. As noted in previous work, most of the absorption features broaden and shift to significantly lower frequency at the higher temperature (295 K). The authors suggest that the THz modes observed are intermolecular (collective) rather than intramolecular in nature since amorphous and aqueous D-glucose lack any sharp features. They also suggested that the spectral differences between D-glucose and D-mannose are a result of changes to the arrangement of hydroxyl groups on the pyranose ring. It is noted that the recent quantum chemical calculations (DFT/PW91) reported by Kawazoe and co-workers[78] using VASP[20] on β-D-glucopyranose monosaccharide crystal[79] may be of particularly relevance to the further interpretation of THz modes of simple sugars.

The two disaccharides investigated consisted of monosaccharides linked by a glycosidic bond. However, the observed THz spectra are entirely different from the constituent monosaccharide spectra. The spectrum for maltose contains at least ten distinct features at 4 K and that of lactose contains three broad features that apparently result from multiple unresolved peaks.

Zhang and co-worker[80] have used THz-TDS to study the dehydration of D-glucose monohydrate. The hydrated sugar was heated at 45 °C for 27 min and a series of spectra covering 0.1–3 THz were taken at 1 min intervals while the sample dehydrated. Absorption peaks of the monohydrate at 1.80 and 1.96 THz decreased over this time while the peaks of the anhydrous sample at 1.28, 1.43 and 2.08 THz increased until the sample was completely dehydrated. From comparison of the integrated absorption peaks in the two samples, the quantity of anhydrous glucose was determined. Of several models tried, the data were best fit to a contracting area equation which describes dehydration as the advancement of a two-phase boundary from the outside crystal surface traveling inward. An Arrhenius plot gave the activation energy of 149 kJ mol^{-1} to dehydration with a correlation coefficient of 0.995.

4.5 Other Small Biomolecules

Walther et al.[81] studied the dielectric function of the biomolecules, benzoic acid, and the monosubstituted analogues, salicylic acid (2-hydroxy-benzoic acid), 3- and 4-hydroxybenzoic acid, and aspirin (acetylsalicylic acid) from 0.5–4.5 THz at 10 K and 300 K using THz-TDS. This series was studied to elucidate the sensitivity of THz vibrational modes to small changes in the overall structure as well as the hydrogen bonding environment. Despite the similarities of the molecular structures, the absorption spectra shared very little in common. The authors attributed modes below 72 cm^{-1} to lattice vibrations and higher frequency resonances to dimer modes (torsions, out-of-plane bends and asymmetric stretches of the hydrogen bonds) based on previous theoretical work.[82] The broadening and red-shift of the features with increasing temperature was attributed to mechanical anharmonicity of the potential energy surfaces. It is further noted that the recent quantum chemical calculations (DFT/PW91) reported by Kawazoe and co-workers[83] using VASP[20] have given a detailed description of the intramolecular verses the lattice vibrational modes of salicylic acid.

Jepsen and co-workers[71] used THz-TDS imaging methods to examine pellet samples of lactose, aspirin, sucrose and tartaric acid at room temperature and developed a recognition coefficient based on unique features that successfully discriminated against these biomaterials. THz-CWS imaging methods have also been successfully applied for detection of illicit drugs[84] and other specific materials.[85]

Similar spectroscopic studies of small pharmaceutical species have also been conducted using THz-TDS by Zeitler et al.[86] Investigations of the spectra below 3 THz were conducted on the active drugs, carbamazepine, piroxicam and theophylline, in the solid state and showed that polymorphism and hydration strongly affected the THz spectrum. This and earlier work by the same group at Teraview in the United Kingdom demonstrated that THz methods can be successfully applied to the study of drug species and that subtle hydration, environmental and structural effects alter drug potency and their controlled manufacture in the pharmaceutical industry.

The impact of mechanical anharmonicity on THz vibrational features was investigated in our group using THz-CWS[11,12] by measuring the temperature dependence of the THz absorption spectrum (0.06-4.3 THz) of crystalline samples of biotin.[87] The THz spectra obtained at 4.2–298 K are shown in Figure 9. A quantitative model was developed to account for observed changes in line shapes and the redistribution of intensity over this temperature range. Such studies are unique to this region since the fundamental vibrational transition frequencies (1 THz $\approx$ 33 cm^{-1}) are comparable to the thermal energy available (kT $\approx$ 200 cm^{-1}) at room temperature. With sufficient spectral resolution ($<$ 0.05 cm^{-1}), the enormous change in the level populations that occur over this temperature range may be exploited to recover upper limits on the mechanical anharmonicity of the vibrational modes. The lower part of Figure 9 illustrates the impact of temperature on the line shape when (positive) mechanical anharmonicity is introduced at the level of 0.1% for a 1 THz vibration.

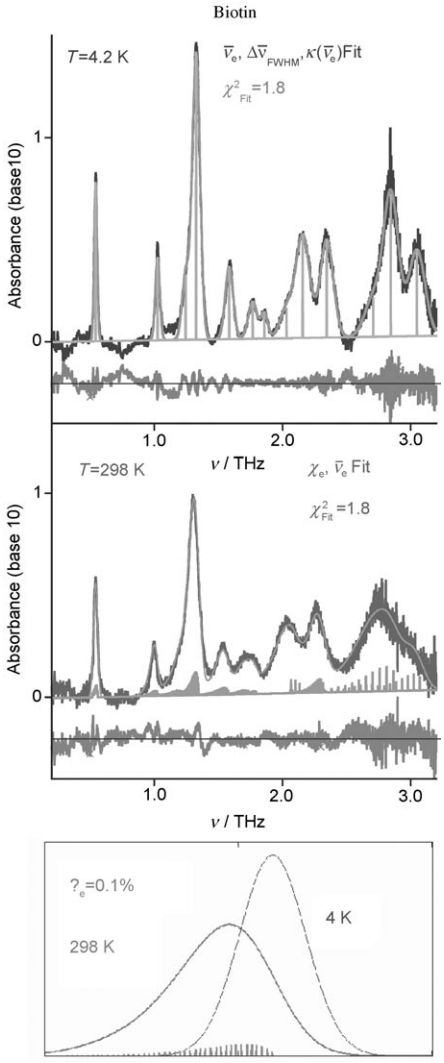

Figure 9. THz absorption spectra (THz-CWS) of crystalline biotin obtained at 4.2 K (top panel) and 298 K (middle panel) where the linearly increasing baseline has been removed. Superimposed on the spectra are model predictions with residuals. The absorption features in the 4.2 K spectrum were first identified and fit to a Gaussian line shape model. The best fit parameters were held fixed in fits to the 298 K spectrum except for the center frequencies and the anharmonicity factors (χ_e). An example of the impact of anharmonicity ($\chi_e = 0.1\,\%$) on the line shape at 1 THz is illustrated at the bottom for the two temperatures.

The model calculations superimposed in Figure 9 were obtained as follows. The 4.2 K spectrum was first least-squares fitted to a Gaussian line shape model containing thirteen lines. The asymmetrically broadened and red-shifted features in the room-temperature spectrum were then fit using just one adjustable parameter per line, the mechanical anharmonicity. This simple model was shown to explain the intensity redistribution and the asymmetric distortion of the line shape at room temperature. With the further relaxation of the center frequencies in the room-temperature fit, the quality of the fit shown in Figure 9 was comparable to that obtained at 4.2 K. Since crystal cage dimensions of peptide crystals are known to vary by 1–3 % over even smaller temperature ranges,[88–93] such shifts are expected based on current theoretical results where the crystal parameters were fully relaxed.

The best-fit Gaussian linewidths obtained at 4.2 K are shown in the top panel of Figure 10 to increase linearly with frequency. The line shape function and linear increase are both consistent with an inhomogeneous broadening mechanism that likely results from the distribution of crystal lattice defects. Consequently, Lorentzian widths arising from vibrational dephasing (or damping) must be less than these widths enabling conservative lower limits on the vibrational lifetimes of 1–5 ps. The anharmonicity factors determined for each line are shown in the lower panel of Figure 10 as a function of frequency and are all positive suggesting the anharmonicity associated with hydrogen bond stretching is more important than negative contributions arising from torsional motions. Moreover, the observed increase with frequency is as expected since the higher frequency modes are likely to have more hydrogen bonding stretch character. The anharmonic constants represent upper limits since contributions from other line broadening factors would only reduce their magnitude. The significance of this study is that it provides quantitative data to assess the impact

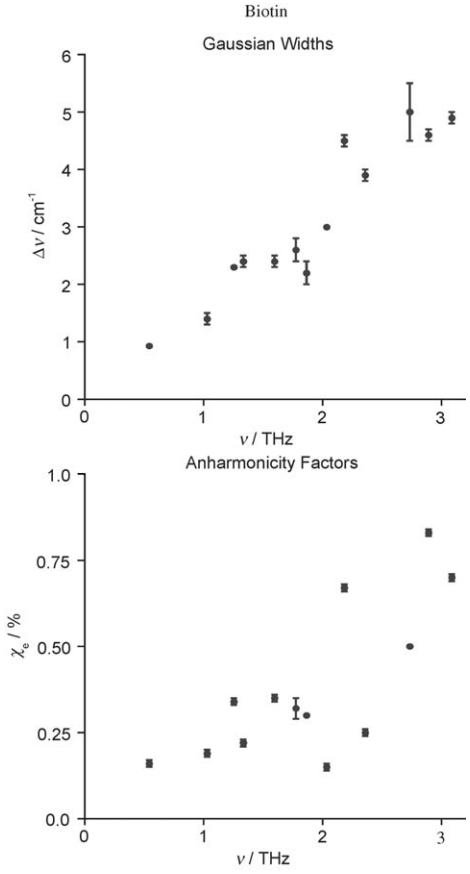

Figure 10. Trends observed in the THz absorption spectra of biotin. In the top panel, the increasing Gaussian linewidths with frequency (observed 4.2 K) is consistent with an inhomogeneous broadening mechanism. In the lower panel, the increasing anharmonicity factors with frequency (obtained from the 298 K spectrum) suggest the vibrational force fields contain increased contributions from hydrogen-bonding stretch potentials.

of anharmonicity on THz spectra and to refine vibrational force field models to better account for the temperature dependence of absorption features.

5. THz Studies of Large Biomolecules

5.1 DNA and RNA

Some of the earliest work on DNA in the THz region (0.09–13.5 THz) was performed by Wittlin et al.[94] over the temperature range from 5–300 K on highly oriented films of DNA salts, Li-DNA and Na-DNA. Five vibrational modes were identified including the lowest frequency modes at 1.35 THz for Li-DNA and 1.23 THz for Na-DNA. These modes were found to red-shift with hydration. A simple lattice dynamical model was reasonably successful in explaining the presence of vibrational modes and the impact of hydration on these modes.

Two artificial RNA single strands composed of polyadenylic acid (*poly-A*) and polycytidylic acid (*poly-C*) were studied by Jepsen and co-workers[95] and Tominaga and co-workers[7] using THz-TDS imaging methods over the frequency range from 0.1–4.0 THz ($\Delta\nu_{Inst} \approx 0.5$ cm^{-1}). The former group recorded images of spotted arrays on a non-polar polymer substrate with densities that varied between $2–7\times10^5$ g mol^{-1} (corresponding to chain lengths of 600–2000 *A* or *C* units). The thin films were formed by dissolving samples in water and by repeated spotting/evaporation of the droplets. A surface profiler was used to character the size of the spots which were 40–50 μm thick with diameters of 1–1.5 mm.

Pressed pellet (bulk) samples were first studied and shown to give unstructured absorption that increased linearly between 0.1–2.5 THz. *Poly-C* was found to absorb more strongly and have a 10% larger refractive index than *poly-A*. Analysis on the thin films was performed by taking the difference in integrated absorption between *poly-A* and *poly-C*. Differences of 10% for 200 μg samples permitted an easy discrimination between these two forms of RNA. Reliable image contrasts were obtained for spot sizes of 1 mm in diameter and for sample weights of ≈100 μg or more. However, they found little discrimination for sample weights of 20 μg. Furthermore, no sharp spectral features were observed for either bulk samples, freestanding thin films or for the spots. They noted that etalon artifacts were largest when the sample absorption was lowest because of multiple bounces between the interfaces. This study contradicts the work of Globus et al.[96,97] discussed below on RNA polymers where structured absorption is reported. Jepsen et al. argue that continuous unstructured absorption is expected in the amorphous condensed phase because of the increasing density of IR-active modes with frequency and the high sensitivity to the local environment where additional damping is expected from random interactions with neighboring molecules. They concluded that the lack of distinct spectral features represents a severe limitation for many biological applications but noted that the careful determination of absorption coefficients could potentially offer additional information about the biomolecule and its environment (see Section 6).

In several papers by Bolivar, Kurz and co-workers,[98,99] THz-TDS has been used for investigations of DNA strand hybridization and as an analytical tool for DNA sequencing. Large differences in the THz absorption upon hybridization were demonstrated, indicating that samples of free strands and hybridized pairs can be readily distinguished.[98] A novel waveguide approach[99] was further developed, enabling direct hybridization with femtomole sensitivity which is of comparable sensitivity to fluorescence tagging methods.

In a series of studies by Hesler, Gelmont, Wollard, Globus and co-workers,[96,97,100–102] THz spectra of single- and double-stranded DNA/RNA samples have been measured using an FTIR spectrometer, typically emphasizing the range from 10–25 cm^{-1} and at resolutions from 0.2–2 cm^{-1}. In an early study of DNA, the Globus and co-workers[96] investigated the THz spectra of four different types of samples: randomly oriented DNA, partially oriented DNA, artificial polynucleotide ribonucleic acid and bacillus subtillis spores. The four sample types were prepared in various manners to achieve a film 50–300 μm thick which was either free-standing or applied to a near-transparent substrate. Intensity variations of typically 1–2%, with a density of ≈1 feature per cm^{-1} are identified as structure on transmission spectra and interpreted as evidence of a high density of IR-active modes. This apparent structure was found to vary depending upon sample thickness and aging characteristics, sample orientation, and water content.

Globus and co-workers[97] also examined the THz spectra of known sequences of single-stranded RNA potassium salts and double-stranded RNA sodium salts. Single strand samples consisted of poly-adenine (A), poly-guanine (G), poly-cytosine (C) and poly-uracile (U) and double-strand samples consisted of paired homopolymers C-G and A-U. Films were prepared with sample concentrations of 2–20% in water. Dried films 1–250 μm thick were either free standing or applied to near-transparent 8 μm thick polycarbonate substrates. Spectral features were again identified at levels of a few percent in overall transmission levels between 50–90% and were sensitive to details of sample preparation and to orientation. The frequency dependent absorption coefficient was determined for the four single-stranded homopolymers and two double-stranded homopolymers and compared with results from theoretical calculations using JUMNA and LIGAND using the FLEX force field.

Additional studies were done by Globus and co-workers[100] on similar films derived from salmon, herring DNA sodium salts, chicken egg ovalbumin, and bacillus subtillis spores and attempts were made to align the film molecules mechanically to give partially oriented films. Polarization of incident THz radiation was normal to this orientation. For DNA and bacillus subtillis, samples in solution were sealed between thin polyethylene films of 10–100 μm thickness. Transmission spectra of the liquid and solid samples were compared. It was again noted the extreme sensitivity of the spectra to sample preparation including thickness, initial concentration in water, rotational orientation, and in particular, drying conditions which impact phase transitions of the DNA liquid-crystal gels. From reflection and transmission spectra, the frequency-dependent index of refraction and absorption coefficient were determined

using an interference spectrometry technique. Transmission spectra of the bacillus subtillis samples increased with frequency from a level of 88% to 96% across the 15 cm^{-1} range and showed intensity fluctuations of the order of 1–2% with widths ≤ 0.5 cm^{-1}. Results for liquid samples of double-stranded DNA showed decreasing absorption from 97% to 92% across this range with ≈ 1% variations. Absorption by single-stranded DNA samples was generally ≈ 20% greater than for double-stranded DNA per unit weight of sample. In addition, discrimination between the native (double-stranded) and denatured (single-stranded) forms of DNA was claimed based on the differences in three absorption features. For both DNA and bacillus subtillis, similarity is found between spectra of solid and liquid samples, but absorption is stronger for the liquid.

Further efforts by Globus and colleagues in determining of absorption coefficients and refractive indices from reflection and transmission spectra of single- verses double-stranded DNA, as well as ovalbumin, were reported for dried film samples.[101] Again absorption by single-stranded salmon DNA was shown to be 20% higher and to be distinguishable from double-stranded salmon DNA by five spectral features.

In a follow-up study,[102] salmon and herring DNA sodium salts suspended in water or in buffer solution at 5–20 wt% concentration were re-examined with THz radiation 80% polarized. DNA gels which form an ordered liquid-crystalline phase were partially aligned by extruding the sample material through a needle. UV absorption spectra and polarized absorption properties were used to characterize samples. For liquid samples, improved sensitivity from increased intensity and sharpness of features (0.3–0.5 cm^{-1}) was reported when compared to the corresponding solid-phase spectra. As in prior work, THz transmission variations of 0.5–2% (occasionally 4%) on overall transmission levels up to 90% were attributed to structure. Discrimination between the native (double-stranded) and denatured (single-stranded) forms of DNA was claimed based on the differences in four absorption features. These same features were also reported to sharpen and increase in intensity for solution samples, changes that are opposite to that expected from inhomogeneous broadening arising from random solvent interactions. Finally, an overall similarity is reported when comparing the THz spectra of herring and salmon DNA and of single- and double-stranded DNA.

Early work in our group using THz-TDS with Roitberg and Markelz[103] reported the THz absorption spectra of calf thymus DNA, bovine serum albumin (BSA—similar to human serum albumin), and type I collagen which have molecular weights of 12 MDa, 66 kDa, and 360 kDa, respectively. Dry samples in polyethylene powder of varying thickness were investigated to assess artificial contributions from sample etalon effects. After scaling for molecular path length, samples of different thickness all showed Lambert–Beer law behavior. For all three biomolecules, broadband absorption spectra devoid of any features were observed at room temperature and for relative humidities (r.h.) of <5%. For DNA and BSA, absorbance increased roughly linearly with frequency over the observed range of 0–60 cm^{-1}, while absorbance for collagen increased at a faster rate. No measurable difference in the spectra of diluted and undiluted samples was found indicating that spectral contributions from the instrument could not be resolved by the 0.7 cm^{-1} resolution. Spectral differences in the two systems studied ensured that the observed data were indeed probing biomolecular signatures.

Both DNA and BSA were investigated under different conditions of relative humidity to study the hydration dependence of the THz response. Pure samples were used to ensure that polyethylene did not hinder sample hydration. Both BSA and DNA exhibited changes in the THz absorbance over the 0–60 cm^{-1} range observed. It was noted that both BSA and DNA are expected to have conformations that depend on the degree of hydration.

DNA has a predominantly helical A conformation at r.h. between 45% and 92% but a disordered helical A conformation at lower hydration and predominantly helical B conformation at higher hydration. Of the three spectra, the first was taken at <5% r.h., the second at 43% r.h. (near the transition point) and the third at 70% r.h. Interestingly, the first and last spectra, corresponding to the disordered and ordered helical A states are distinctly different, while the second spectrum near the transition point shares features from both.

5.2 Proteins

In the second part of our work with Roitberg and Markelz,[103] we examined bovine serum albumin and type I collagen. The conformation of BSA as a function of hydration is not definitively known but is expected to be similar to human serum albumin. The latter has a greater content of β-sheet conformation for r.h. <16% but increasing α-helical content for 30–50% r.h. The spectrum observed for BSA at <5% r.h. was similar to that of denatured BSA but red-shifted while the spectrum observed for BSA at 77% r.h. showed some differences including an increased red-shift. These differences may reflect the expected changes from β-sheet to α-helix in the conformational composition of the sample.

An important aspect of sample preparation is the time for structural equilibration which may take several days after conditions of humidity are changed. The samples studied here, however, were exposed for only 90 min prior to the acquisition of spectra. Therefore, it is not possible with any certainty to attribute the changes observed in the THz spectra to the conformation changes expected for equilibrium hydration levels. In light of our more recent work on crystalline dipeptides[56,57] and tripeptides,[65] equilibrium times can range from hours to days and structurally integrated water, non-hydrogen bonded water or superficially adsorbed water can have widely varying impacts on the THz response.

The three different retinal isomers that occur in the photoactive proteins, rhodopsin, bacteriorhodopsin and isorhodopsin were investigated by Jepsen and co-workers[104] between 10–100 cm^{-1} at 10 K and room temperature. The three different crystalline forms prepared in polyethylene pellets included the all-*trans*, 9-*cis* and 13-*cis* isomers that differ only in their conformational structure. The absorption data illustrate the utility of this spectral region for the clear distinction of isomeric sam-

ples. Furthermore, the broad absorption features present at room temperature are shown to sharpen and blue-shift with decreasing temperature.

Based on fits of the 10 K data to a frequency-dependent complex dielectric function, the center frequencies, linewidths, and oscillator strengths (and integrated band intensities) are reported for the three isomers. For the all-*trans* form, these same parameters are used to model the room-temperature data after red-shifting all frequencies by 4.5 cm^{-1} and increasing linewidths by a factor of two. Comparison of the absorption features of the three forms enabled some speculation on the types of nuclear motions involved.

The Markelz group in collaboration with Whitmire, Hillebrecht and Birge[105] have gone on to investigate several other proteins using THz-TDS including hen egg white lysozyme, horse heart myoglobin and bacteriorhodopsin. Lysozyme and myoglobin powder were diluted with PE powder and pressed into pellet form. Samples were temperature and humidity controlled and spectra were acquired at 77 K and room temperature. For both substances, broadband absorption without identifiable peaks was observed to increase from 5–40 cm^{-1} and then leveled off near 80 cm^{-1}. At 77 K, absorption was less than at room temperature across the observed spectrum but remained featureless. To confirm the featureless properties of these samples, the THz spectrum of the organic semiconductor, α-hexathiophane, in crystalline form was acquired using an FTIR instrument.

The experimentally measured spectra were compared to the density of normal modes calculated by CHARMm without accounting for oscillator strengths. These calculations were performed on the myoglobin and lysozyme structures available from the protein database without any additional water. The mode density for both samples was roughly 500 modes in the first 80 cm^{-1} with an average separation of 0.2 and 0.16 cm^{-1} for lysozyme and myoglobin, respectively. In both cases, the density of normal modes increased roughly linearly with frequency and leveled off near 60 cm^{-1} in contrast to the experimentally observed maximum absorbance near 40 cm^{-1}. This similarity between the calculated mode density (unweighted by oscillator strength) and observed THz absorption spectra suggested that all modes are IR-active and oscillator strength is not a strong function of frequency. However, from CHARMm and quantum chemical calculations on small crystalline systems, unphysical results were found for these simple systems without a high degree of verisimilitude in the model to mimic the surrounding molecular environment. In particular, without the environment, the optimized geometry was not consistent with the known geometry. Furthermore, results employing periodic boundary conditions were still unsatisfactory. While the mode density predicted by CHARMm was roughly correct, the positions and intensities of lines could not be reconciled with experimental data.

Markelz in collaboration with Whitmire, Hillebrecht, Birge and others[106] reported the first demonstration of THz response to conformational state in some interesting and well-conceived studies of bacteriorhodopsin (BR). BR undergoes a light activated photocycle consisting of a series of intermediate conformational states labeled K through O which are all identifiable by their UV/Vis absorption spectra. The end result of the photoisomerization processes and the interactions between the chromophore and its binding pocket enabled by conformational changes is the transport of a proton from the inner to the outer side of the cell membrane which generates a potential gradient to drive formation of ATP. In this photocycle, the particular conformation state labeled M has the useful property that its 10 ms lifetime can be prolonged indefinitely at 233 K. Hence, under appropriate conditions of humidity, the M state can be photo-induced at wavelengths <570 nm and then captured at 233 K to permit the THz spectra to be measured and compared with the spectrum of the ground state conformation.

This work investigated two forms of BR, the wild type (WT) and the D96N mutant, which involves a single residue change. In the D96N mutant, the 96th aspartic acid residue of the 248-residue chain is replaced by asparagine. This seemingly small change of structure results in a 1000-fold increase in the photocycle time of the molecule.[107] It has been suggested that this increase is due to the loss of conformational flexibility with mutation. Differences in THz response between the WT and mutant BR may therefore suggest a possible correlation with conformational flexibility since motions permitting conformational state transitions may be decomposed into a series of THz vibrational motions. Hence, conformational transitions requiring access to the lowest frequency collective modes may impact the THz response.

The THz absorption spectra of the two types of BR were first obtained at 80% relative humidity (r.h.) and room temperature for 200 μm thick films on infrasil quartz substrates. In both cases, absorption over the range 0–60 cm^{-1} is broad and increases linearly with frequency but the absorption of the D96N is lower by a factor of 1.8. No difference was observed in spectra taken at 30% r.h. but at <5% r.h., absorption in both species decreased markedly. The change was too large to be explained by mass-loading effects of water content and may result from intramolecular coupling effects and/or collective modes of interior water clusters.

The normal mode frequencies and eigenvectors derived from CHARMm were calculated to verify that indeed the very lowest frequency modes were responsible for the largest structural fluctuations while higher frequency modes involved only smaller rms fluctuations. Additional calculations performed for both WT and D96N utilized the approximation that the transition dipole moment is proportional to its derivative with respect to the normal mode coordinate. Absorption was then estimated using an ad hoc method to account for anharmonicity with no explicit reference to temperature. Some agreement was found in comparisons with the initial BR spectra taken at room temperature and 80% r.h. However, little difference was found between the calculated spectra of the WT and mutant BR in contrast to the large differences observed experimentally.

In studies comparing illuminated and non-illuminated BR, the THz spectra were first obtained at room temperature for the ground state and then again after cooling to 233 K. For WT-BR, the broadband featureless absorption decreased mark-

edly with decreasing temperature at the upper end of the 0–60 cm^{-1} range. Conversely, absorption decreased in D96N-BR with decreasing temperature at the lower frequencies in the range. The most striking effect occurred, however, upon the photo-conversion to the M state at 233 K where the THz absorption increased relative to that at room temperature. In contrast, the absorption strength remained essentially unchanged in D96N-BR after conversion from the ground state to the M state. On illumination with <480 nm light, the THz response of WT-BR reverted to that previously observed for the ground state at 233 K and at room temperature. A change in M state absorbance can result from either a change in transition dipole moment or a change in the distribution of normal modes. Since the former differences are nearly identical for both WT and D96N, a greater increase in normal mode density for WT with conformational change was suggested to explain the THz response. However, it should be noted that the UV/Vis spectra used to confirm conformation state indicated a lower M state content for illuminated WT-BR at 233 K than for illuminated D96N-BR at 233 K. Therefore, the presence of N or P states in illuminated WT-BR might conceivably be responsible for the observed absorption increase.

The significance of these results is the demonstration of the sensitivity of the THz response to changes in conformation state as well as to changes of a single residue in the peptide sequence. These studies also raise unanswered questions relating to the quality of theoretical models. The CHARMm results showed no obvious basis for the lower THz absorption of D96N-BR in the ground state compared to WT-BR, nor explained the striking difference in the THz response of WT-BR compared to mutant D96N BR under illumination and conformation change. It is important to note that the CHARMm calculations contained no bound water while our studies on crystalline peptides[56,57,65] have shown that water can strongly impact the THz spectra. These studies have also suggested that the harmonic approximation may not be adequate to reproduce finer details of the observed THz spectra.

Tominaga and co-workers[7] were first to report on the THz spectrum of cytochrome C (CytC), a string of 104 amino acids having a covalently bonded heme group. In more recent work, Markelz and co-workers[107] have also reported on CytC using THz-TDS. CytC is an electron transfer protein that has two forms which are structurally quite similar yet have quite different thermal stabilities, hydrogen atom exchange rates and proteolytic digestion rates. The bound heme group exists in two oxidation states and X-ray measurements, NMR structural measurements, and compressibility measurements have indicated that the oxidated state (which is the less stable and more active state) has greater conformational flexibility than the reduced state in spite of their great structural similarity.

In the study by Markelz and co-workers,[107] the THz absorption coefficient of the oxidized state was observed to be much greater than that of the reduced state. Furthermore, the THz response was broad, essentially featureless, and aptly characterized as "glass-like" over the 10–80 cm^{-1} range measured. To fit the dielectric response, it was assumed that all modes were IR-active and have uniform oscillator strengths across the observed frequency range. Differences in the fits were suggested to arise from differences in dipole coupling strength and/or mode density. However, the predicted dipole moment difference between the oxidized and reduced state was only about 6% and the observed difference in response was too large to be explained by an increased mode density resulting from the higher water content of the oxidized state. These outcomes were most consistent with an increased number of low frequency modes for the oxidized state and illustrated the use of THz spectra as a measure of the accessibility of the low frequency modes crucial to conformational flexibility.

In the most recent work by Markelz and co-workers,[108] the THz response of hen egg white lysozyme was investigated as a function of hydration for r.h. from 3–39%. Other workers using NMR, specific heat, and microwave spectroscopic measurements have previously identified a transition point near 27% r.h. at which point the first hydration shell is filled and bulk water begins to accumulate. Evidence of this transition was also seen in this work for which very uniform thin films ($\approx$100 μm thick) of lysozyme were prepared on quartz substrates. The lysozyme samples were allowed to reach equilibrium in a humidity-controlled cell at room temperature prior to obtaining spectra.

For lysozyme, the absorption coefficient increased nearly linearly with frequency and the index of refraction was nearly constant for all levels of hydration. Of particular interest was the sudden increase in the entire absorption curve at 27% r.h. and the larger subsequent curve shifts as hydration increased. A similar effect was seen for the refractive index at the same transition point. The apparent discontinuities were indicative of a transition from the occupation of bound water sites to bulk water accumulation.

In previous work on large biomolecules, CHARMm calculations were used to predict the normal mode distribution and then the THz response was estimated after making simplifying assumptions about the transition dipole strengths. In this study, a new approach was taken to model the THz response based on conformational lifetimes since the system at room temperature is likely composed of multiple conformations. Several such models were investigated but results were not entirely satisfactory. Simple one- or two-relaxation time models gave reasonably good fits to the observed data but unfortunately unrealistically short lifetimes compared to relaxation times experimentally determined by others. On the other hand, good fits could be obtained by adding a sufficient number of relaxation times and oscillators but the physical reason for such a model could not be justified.

5.3 Polysaccharides

In a few studies, the naturally occurring long range order of polysaccharides and related biopolymers was investigated in the THz region. Cellulose, for example, is a hydrogen-bonded triple helix with each strand composed of polyglucose units. The THz spectrum of cellulose was measured in our group using THz-FTIR (unpublished). The THz absorption (and inelastic neutron scattering) spectra of purified cellulose powder is

shown in Figure 11. There are clear absorption and scattering features that occur at 3, 5, 7, 9 and 11 THz. While there are no modeling results for this system, it is surmised that the periodicity of these systems probably produces inter-strand twisting or stretching motions that show up as harmonics in the THz spectrum. Further studies of modified cellulose (with different crystalline forms or substituted forms such as nitrocellulose) are clearly warranted as are DFT periodic system calculations to help identify the origin of these unique polymeric spectral features.

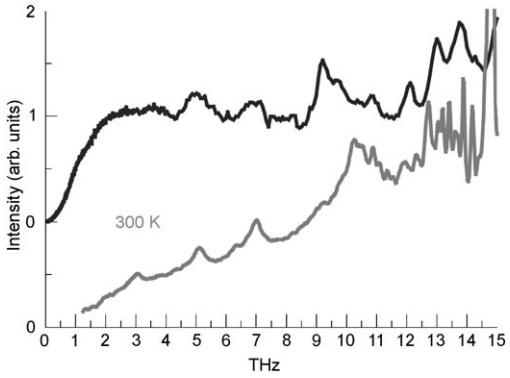

Figure 11. Inelastic neutron spectrum (top) and THz absorption spectrum (bottom) for dispersed cellulose powder in polyethylene matrix. The triple-helix polymer exhibits distinct positive absorption features at 1, 3, 5, 7, 9 THz and higher frequencies, presumably arising from internal collective motions of the helix.

Jepsen and co-workers[71] examined cellulose and chitin using THz-TDS and found that absorption features absent at 300 K appeared on a broad absorption background when cooled to 10 K. These features were attributed to absorption by one-dimensional phonon-like modes along the backbone of the polymers.

6. THz Studies of Biomolecules in Liquid Water

Several recent studies (published at nearly the same time) have addressed the use of THz spectroscopy to probe biomolecules in aqueous environments. For example, the Havenith group[109] found that the THz region provides a sensitive probe of solute-induced changes in water's hydrogen bonding network near the vicinity of a biomolecule. The simple sugar, lactose, has been investigated using *p*-Ge-laser THz source[110] over the spectral region from 2.3 THz and 2.9 THz. Highly accurate absorption measurements were performed on bulk water and lactose powder and compared with total absorption measured for a series of different concentrations of lactose in water. The challenge of these measurements arises because the absorption coefficient of water is 450 cm^{-1} at 3 THz and therefore, measurements were performed in a cell 150 μm in length. Absorption for solutions was found to be greater than the fractional sum (by volume) of the bulk absorptions. This difference amounted to 65% of the total absorption for 0.7 mol l^{-1} solution. Further measurements of volume and modeling of hydration shells indicated the solute induced perturbations extended more than 5 Å from the surface of lactose. This volume corresponds to 123 water/lactose molecule. Simulations using molecular mechanics (and the CHARMm force field) reveal a slowing down of the hydrogen bond rearrangement dynamics in the hydration spheres. This study demonstrates that THz spectroscopy probes the coherent solvent dynamics on the sub-ps time scale and gives quantitative measure of the extent the solute influences biological water (i.e. water near the surface of a biomolecule).

In a THz study (0.1–1.2 THz) of myoglobin (Mb) using THz-TDS, Durbin and Zhang[111] reported an increase in the absorption per protein molecule in the presence of "biological" water. Absorption measurements were made on samples between 3.6 wt% to 90 wt% water[112] as confirmed by weight loss upon heating and accurate optical pathlength determinations critical to this analysis were determined from comparisons made using 100 μm and 200 μm cuvettes. As with the other large biomolecules described above, nearly continuous broadband absorption that increased linearly with frequency was observed. However, deviations of the normalized absorption from an idealized non-interacting Mb-water model showed enhanced THz absorption rather than a reduction expected on theoretical grounds (from a decrease in the 2.5 Debye moment of bulk water to 0.8 Debye because of hindered motions experienced by biological water). The increased absorption and hence, polarizability of Mb across the THz region (especially above 90 wt% water) was suggested to result from the enhanced mobility of the side chains along the protein[113] and for >90 wt% water, increased rotational freedom of Mb that occurs when the average separation (>6 nm) becomes significantly larger than radius of gyration (1.5 nm).

Allen and co-workers[114] reexamined bovine serum albumen using a free electron laser source from 0.3–3.72 THz and compared their results to those of Markelz below ≈ 1 THz. While agreement was found to within the error bars for dry BSA, the absorption was larger at higher frequencies for the solute BSA than for dry sample. The extinction coefficient of the protein in a concentrated aqueous solution (27% BSA) was separated into contributions from the two components, water and protein. Because of discrepancies in this sum, modeling results were used to predict the water content expected in the hydration layer. From this analysis, absorption by the bound water plus protein was determined.

In the second paper on lysozyme, Allen and co-workers[115] note that at very low frequencies (≈ 3 cm^{-1}), absorption predicted for bulk water was higher than that of the solution. The difference was used to estimate the amount of bound water that was not contributing to bulk water absorption. This measure of bound water agreed with other experimental measurements on lysozyme.[108] Furthermore, reasonable agreement was found between the observed molar extinction and the normal mode density calculated by Markelz and co-workers[108] and by others.[116] It was further noted that the molar extinction of BSA continued to increase with frequency but for lyso-

zyme, it leveled off at 2 THz. However, the experimental absorption curves were more similar if the extinction coefficients were normalized on a per residue basis (BSA is 66.4 kDa versus 14.3 kDa for lysozyme).

The significance of these latter studies is that through quantitative THz absorption measurements, the solvent–biomolecule interfacial structure and dynamics may be examined directly.

7. Future Prospects

We have attempted to give an overview of the impressive achievements realized in the field of THz spectroscopy of biomolecules as reflected by the large body of data initially available and the numerous contributions witnessed during the preparation of this article. Given the breadth of this field, we apologize for references to studies relevant to biomolecular applications missed in this review. As exemplified by the wide range of biosamples investigated, recent technological advances made with THz sources, detectors and techniques have enabled key finding in areas ranging from structural biology of crystalline solids to solvation dynamics of hydrated and aqueous samples. With that said, much more work needs to be done to further stimulate a wider range of interest and participation in this field by others in the biocommunity.

With the ever increasing accuracy of spectroscopic data reported in the THz region, perhaps one of the greatest hurdles to overcome is in the state of the theoretical models necessary to interpret these results. Nowhere is this more apparent than in comparisons with data from the well-ordered environments of crystalline solids. Even when the structural framework is unambiguous, quantum chemical calculations are often not of sufficient accuracy to predict the nuclear motions responsible for features in this region. As seen from the examples cited here, these discrepancies appear to become increasing problematic as the energy landscape softens and approaches an aqueous-like environment.

In the mid-IR region, the synergistic relationship between gas phase vibrational spectroscopy and theory has provided the impetus for major advances in understanding the conformational preferences of small peptides[117–120] and nucleic acid base pairs.[121] Together with the growing body of THz data on crystalline solids, it is anticipated that further improvements in density functionals and theories will soon become available. However, for the newest THz data emerging from the most relevant biochemical studies where system size and aqueous environment prohibit the application of quantum chemical methods, classical and semi-classical models offer the only hope for qualitative interpretation and insight into the biomolecular dynamics of these systems. Bridging the gap between the quantum and classical limits with particular emphasis on the refinement of water models is yet another major challenge facing the field with substantial improvements anticipated to result from experimental and quantum chemical feedback. As these advances are realized, THz spectroscopy will find increasing applications in a wide range of biosystems.

Acknowledgements

We wish to thank all of our NIST colleagues, postdoctoral associates, guest researchers and students for their participation in the THz spectroscopy work reviewed herein. Without their efforts, research prowess, and attention to detail the results we provided to the scientific community over the last thirteen years would not have been possible.

Keywords: biophysics · density functional calculations · structure elucidation · terahertz spectroscopy · vibrational spectroscopy

[1] R. H. Callender, R. B. Dyer, R. Gilmanshin, W. H. Woodruff, *Annu. Rev. Phys. Chem.* **1998**, *49*, 173.
[2] W. A. Eaton, V. Munoz, S. J. Hagen, G. S. Jas, L. J. Lapidus, E. R. Henry, J. Hofrichter, *Annu. Rev. Biophys. Biomol. Struct.* **2000**, *29*, 327.
[3] S. Takahashi, S. R. Yeh, T. K. Das, C. K. Chan, D. S. Gottfried, D. L. Rousseau, *Nat. Struct. Biol.* **1997**, *4*, 44.
[4] D. M. Leitner, M. Havenith, M. Gruebele, *Int. Rev. Phys. Chem.* **2006**, *25*, 553.
[5] A. G. Markelz, A. Roitberg, E. J. Heilweil, *Chem. Phys. Lett.* **2000**, *320*, 42.
[6] R. Nossal, H. Lecar, *Molecular and Cell Biophysics, 1st ed.*, Addison-Wesley, Redwood City, **1991**.
[7] K. Yamamoto, K. Tominaga, H. Sasakawa, A. Tamura, H. Murakami, H. Ohtake, N. Sarukura, *Bull. Chem. Soc. Jpn.* **2002**, *75*, 1083.
[8] J. T. Kindt, C. A. Schmuttenmaer, *J. Phys. Chem.* **1996**, *100*, 10373.
[9] B. S. Hudson, *J. Phys. Chem. A* **2001**, *105*, 3949.
[10] A. S. Pine, R. D. Suenram, E. R. Brown, K. A. McIntosh, *J. Mol. Spectrosc.* **1996**, *175*, 37.
[11] D. F. Plusquellic, T. M. Korter, G. T. Fraser, R. J. Lavrich, E. C. Benck, C. R. Bucher, J. Domench, A. R. Hight Walker in *Terahertz Sensing Technology. Vol. 2: Emerging Scientific Applications and Novel Device Concepts* (Eds.: D. L. Wollard, W. R. Loerop, M. S. Shur), World Scientific, New Jersey, **2003**, p. 385.
[12] T. M. Korter, D. F. Plusquellic, *Chem. Phys. Lett.* **2004**, *385*, 45.
[13] K. A. McIntosh, E. R. Brown, K. B. Nichols, O. B. McMahon, W. F. DiNatale, T. M. Lyszczarz, *Appl. Phys. Lett.* **1995**, *67*, 3844.
[14] C. Kadow, S. B. Fleischer, J. P. Ibetzon, J. E. Bowers, A. C. Gossard, J. W. Dong, C. J. Palmstrom, *Appl. Phys. Lett.* **1999**, *75*, 3548.
[15] M. C. Beard, G. M. Turner, C. A. Schmuttenmaer, *J. Phys. Chem. B* **2002**, *106*, 7146.
[16] O. Esenturk, A. Evans, E. J. Heilweil, *Chem. Phys. Lett.* **2007**, *442*, 71.
[17] Certain commercial equipment, instruments, or materials are identified in this paper to adequately specify the experimental procedure. In no case does identification imply recommendation or endorsement by NIST, nor does it imply that the materials or equipment identified are necessarily the best available for the purpose.
[18] G. M. Day, J. A. Zeitler, W. Jones, T. Rades, P. F. Taday, *J. Phys. Chem. B* **2006**, *110*, 447.
[19] R. Dovesi, V. R. Saunders, C. Roetti, R. Orlando, C. M. Zicovich-Wilson, F. Pascale, B. Civalleri, K. Doll, N. M. Harrison, I. J. Bush, Ph. D'Arco, M. Llunell, See: http://www.crystal.unito.it/.
[20] G. Kresse, D. Joubert, *Phys. Rev. B* **1999**, *59*, 1758.
[21] S. J. Clark, M. D. Segall, C. J. Pickard, P. J. Hasnip, M. J. Probert, K. Refson, M. C. Payne, *Z. Kristallogr.* **2005**, *220*, 567.
[22] M. J. Frisch, G. W. Trucks, H. B.Schlegel, G. E. Scuseria, M. A. Robb, J. R. Cheeseman, V. G. Zakrzewski, J. A. Montgomery, Jr., R. E. Stratmann, J. C. Burant, S. Dapprich, J. M. Millam, A. D. Daniels, K. N. Kudin, M. C. Strain, O. Farkas, J. Tomasi, V. Barone, M. Cossi, R. Cammi, B. Mennucci, C. Pomelli, C. Adamo, S. Clifford, J. Ochterski, G. A. Petersson, P. Y. Ayala, Q. Cui, K. Morokuma, P. Salvador, J. J. Dannenberg, D. K. Malick, A. D. Rabuck, K. Raghavachari, J. B. Foresman, J. Cioslowski, J. V. Ortiz, A. G. Baboul, B. B. Stefanov, G. Liu, A. Liashenko, P. Piskorz, I. Komaromi, R. Gomperts, R. L. Martin, D. J. Fox, T. Keith, M. A. Al-Laham, C. Y. Peng, A. Nanayakkara, M. Challacombe, P. M. W. Gill, B. Johnson, W. Chen, M. W. Wong, J. L. Andres, C. Gonzalez, M. Head-Gordon, E. S. Re-

plogle, J. A. Pople, Gaussian 98 (Revision A.11.3), Gaussian, Inc., Pittsburgh PA, **2001**.
[23] See: http://webbook.nist.gov/chemistry.
[24] A. D. MacKerell, N. Banavali, N. Foloppe, *Biopolymers* **2000**, *56*, 257.
[25] B. R. Brooks, R. E. Bruccoleri, B. D. Olafson, D. J. States, S. Swaminathan, M. Karplus, *J. Comput. Chem.* **1983**, *4*, 187.
[26] R. B. Gerber, C. M. Chaban, S. K. Gregurick, B. Brauer, *Biopolymers* **2003**, *68*, 370.
[27] S. K. Gregurick, S. A. Kafafi, *J. Carbohydr. Chem.* **1999**, *18*, 867.
[28] M. M. Harding, H. A. Long, *Acta Crystallogr. Sect. B* **1968**, *24*, 1096.
[29] B. Khawas, *Acta Crystallogr. Sect. B* **1971**, *27*, 1517.
[30] T. J. Kistenmacher, G. A. Rand, R. E. Marsh, *Acta Crystallogr. Sect. B* **1974**, *30*, 2573.
[31] C. H. Görbitz, B. Dalhus, *Acta Crystallogr. Sect. C* **1996**, *52*, 1756.
[32] M. N. Frey, M. S. Lehman, T. F. Koetzle, W. C. Hamilton, *Acta Crystallogr. Sect. B* **1973**, *29*, 876.
[33] K. A. Kerr, J. P. Ashmore, T. F. Koetzle, *Acta Crystallogr. Sect. B* **1975**, *31*, 2022.
[34] P. Ewald, *Ann. Phys.* **1921**, *64*, 253.
[35] U. Essmann, L. Perera, M. L. Berkowitz, T. Darden, H. Lee, L. G. Pedersen, *J. Chem. Phys.* **1995**, *103*, 8577.
[36] W. A. Majewski, J. F. Pfanstiel, D. F. Plusquellic, D. W. Pratt, *Laser Techniques in Chemistry, Vol. XXIII* (Eds.: A. B. Myers, T. R. Rizzo), Wiley, New York, **1995**, pp. 101 – 148; D. F. Plusquellic, R. D. Suenram, B. Mate, J. O. Jensen, A. C. Samuels, *J. Chem. Phys.* **2001**, *115*, 3057.
[37] R. Car, M. Parrinello, *Phys. Rev. Lett.* **1985**, *55*, 2471.
[38] N. Trouiller, J. L. Martins, *Phys. Rev. B* **1991**, *43*, 1943.
[39] L. Kleinman, D. M. Bylander, *Phys. Rev. Lett.* **1982**, *48*, 1425.
[40] R. Resta, *Phys. Rev. Lett.* **1998**, *80*, 800.
[41] D. A. McQuarrie, *Statistical Mechanics*, Harper-Collins, New York, **1976**.
[42] B. Delley, *J. Chem. Phys.* **2000**, *113*, 7756.
[43] J. P. Perdew, Y. Wang, *Phys. Rev. B* **1992**, *45*, 13244.
[44] O. Esenturk, B. Sheinman, E. J. Heilweil, unpublished results.
[45] F. H. Herbstein, M. Kapon, *Acta Crystallogr. Sect. B* **1990**, *46*, 567.
[46] J. Melinger, N. Laman, S. Sree Harsha, D. Grischkowsky, *Appl. Phys. Lett.* **2006**, *89*, 251110.
[47] M. Kutteruf, C. Brown, L. Iwaki, M. Campbell, T. A. Korter, E. J. Heilweil, *Chem. Phys. Lett.* **2003**, *375*, 337.
[48] T. M. Korter, R. Balu, M. B. Campbell, M. C. Beard, S. K. Gregurick, E. J. Heilweil, *Chem. Phys. Lett.* **2006**, *418*, 65.
[49] R. Rungsawang, Y. Ueno, I. Tomita, K. Ajito, *J. Phys. Chem. B* **2006**, *110*, 21259.
[50] M. Yamaguchi, F. Miyamaru, K. Yamamoto, M. Tani, M. Hangyo, *Appl. Phys. Lett.* **2005**, *86*, 053903.
[51] B. M. Fischer, M. Franz, D. Abbott, *Proceedings of SPIE: Biomedical Applications of Micro- and Nanoengineering III*, **2006**, 6416, 64160U.
[52] R. Balu, S. K. Gregurick, E. J. Heilweil, unpublished results.
[53] C. H. Görbitz, *Acta Crystallogr. Sect. B* **2002**, *58*, 849.
[54] C. H. Görbitz, *New J. Chem.* **2003**, *27*, 1789.
[55] C. H. Görbitz, E. Gundersen, *Acta Crystallogr. Sect. C* **1996**, *52*, 1764.
[56] "New Approaches in Biomedical Spectroscopy": K. Siegrist, C. R. Bucher, C. Pfefferkorn, A. Schwarzkopf, D. F. Plusquellic, *ACS Symp. Ser.* **2007**, *963*, 280.
[57] K. Siegrist, D. F. Plusquellic, unpublished results.
[58] R. Mendis, D. Grischkowsky, *Opt. Lett.* **2001**, *26*, 846.
[59] J. Zhang, D. Grischkowsky, *Opt. Lett.* **2004**, *29*, 1617.
[60] N. Laman, S. Sree Harsha, D. Grischkowsky, J. S. Melinger, *Conference on Lasers and Electro-Optics* **2007**, OSA Technical Digest CD-ROM, paper CFS4.
[61] D. F. Plusquellic, I. Kleiner, J. Demaison, R. D. Suenram, R. J. Lavrich, F. J. Lovas, G. T. Fraser, V. V. Ilyushin, *J. Chem. Phys.* **2006**, *125*, 104312.
[62] R. J. Lavrich, A. R. Hight Walker, D. F. Plusquellic, I. Kleiner, R. D. Suenram, J. T. Hougen, G. T. Fraser, *J. Chem. Phys.* **2003**, *119*, 5497.
[63] R. J. Lavrich, D. F. Plusquellic, R. D. Suenram, G. T. Fraser, A. R. Hight Walker, M. J. Tubergen, *J. Chem. Phys.* **2003**, *118*, 1253.
[64] D. F. Plusquellic, D. W. Pratt, *J. Phys. Chem. A* **2007**, *111*, 7391.
[65] K. Siegrist, C. R. Bucher, I. Mandelbaum, A. R. Hight Walker, R. Balu, S. K. Gregurick, D. F. Plusquellic, *J. Am. Chem. Soc.* **2006**, *128*, 5764.
[66] A. Hempel, N. Camerman, A. Camerman, *Biopolymers* **1991**, *31*, 187; J. K. Fawcett, N. Camerman, A. Camerman, *Acta. Crystallogr. Sect. B.* **1975**, *31*, 658.
[67] M. Yamaguchi, K. Yamamoto, M. Tani, M. Hangyo, *IEEE Conference Proceedings on Biological and Medical Applications, Ultrafast Chemistry and Physics*, *13th Int. Conf. on Infrared and Millimeter Waves* **2005**, WB3-3, 477.
[68] W. Qian, J. Bandekar, S. Krimm, *Biopolymers* **1991**, *31*, 193.
[69] Z. Bihary, R. B. Gerber, *J. Chem. Phys.* **2001**, *115*, 2695.
[70] B. M. Fischer, M. Walther, P. U. Jepsen, *Phys. Med. Biol.* **2002**, *47*, 3807.
[71] B. Fischer, M. Hoffmann, H. Helm, G. Modjesch, P. Uhd Jepsen, *Semicond. Sci. Technol.* **2005**, *20*, S246.
[72] Y. C. Shen, P. C. Upadhya, E. H. Linfield, A. G. Davies, *Vib. Spectrosc.* **2004**, *35*, 111.
[73] M. Walther, B. M. Fischer, P. Uhd Jepsen, *Chem. Phys.* **2003**, *288*, 261.
[74] Y. C. Shen, P. C. Upadhya, E. H. Linfield, *Appl. Phys. Lett.* **2003**, *82* 2350.
[75] Y. C. Shen, P. C. Upadhya, E. H. Linfield, *Appl. Phys. Lett.* **2005**, *87*, 011105.
[76] J. Kröll, J. Darmo, K. Unterrainer, *Vib. Spectrosc.* **2007**, *43*, 324.
[77] P. C. Upadhya, Y. C. Shen, A. G. Davies, E. H. Linfield, *Vib. Spectrosc.* **2004**, *35*, 139.
[78] S. Saito, T. M. Inerbaev, H. Mizuseki, N. Igarashi, R. Note, Y. Kawazoe, *Chem. Phys. Lett.* **2006**, *423*, 439.
[79] M. Hineno, *Carbohydr. Res.* **1977**, *56*, 219.
[80] H.-B. Liu, X.-C. Zhang, *Chem. Phys. Lett.* **2006**, *429*, 229.
[81] M. Walther, P. Plochocka, B. M. Fischer, H. Helm, P. U. Jepsen, *Biopolymers* **2002**, *67*, 310.
[82] H. R. Zelsmann, Z. Mielke, *Chem. Phys. Lett.* **1991**, *186*, 501.
[83] S. Saito, T. M. Inerbaev, H. Mizuseki, N. Igarashi, Y. Kawazoe, *Jpn. J. Appl. Phys. Part 1* **2006**, *45*, 4170.
[84] K. Kawase, Y. Ogawa, Y. Watanabe, H. Inoue, *Opt. Express* **2003**, *11*, 2549.
[85] T. Watanabe, K. Kawase, T. Ikari, H. Ito, Y. Ishikawa, H. Minanide, *Appl. Phys. Lett.* **2003**, *83*, 800.
[86] J. A. Zeitler, K. Kogermann, J. Antanen, T. Rades, P. F. Taday, M. Pepper, J. Aaltonen, C. J. Strachan, *Int. J. Pharm.* **2007**, *334*, 78.
[87] D. G. Allis, A. M. Fedor, T. M. Korter, J. E. Bjarnason, E. R. Brown, *Chem. Phys. Lett.* **2007**, *440*, 203.
[88] B. Dalhus, C. H. Gorbitz, *Acta Chrystallogr. Sect. C* **1996**, *52*, 1759.
[89] B. Dawson, A. Mathieson, *Acta Chrystallogr.* **1951**, *4*, 475.
[90] W.-Q. Wan, Y. Gong, Z.-M. Wang, C.-H. Yan, *Chin. J. Struct. Chem.* **2003**, *22*, 539.
[91] B. Dalhus, C. H. Gorbitz, *Acta Chem. Scand.* **1996**, *50*, 544.
[92] W. Q. Wang, Y. Gong, Z. Liang, F. L. Sun, D. X. Shi, H. J. Gao, X. Lin, P. Jiang, Z. M. Wang, *Surf. Sci.* **2002**, *512*, 379.
[93] K. Tori, Y. Iitaka, *Acta Crystallogr. Sect. B* **1970**, *26*, 1317.
[94] A. Wittlin, L. Genzel, F. Kremer, S. Haseler, A. Poglitsch, *Phys. Rev. A* **1986**, *34*, 493.
[95] B. M. Fischer, M. Hoffmann, H. Helm, R. Wilk, F. Rutz, T. Kleine-Ostmann, M. Koch, P. U. Jepsen, *Opt. Express* **2005**, *13*, 5205.
[96] T. Globus, D. L. Woolard, A. C. Samuels, B. L. Gelmont, J. Hesler, T. W. Crowe, M. Bykhovskaia, *J. Appl. Phys.* **2002**, *91*, 6105.
[97] T. Globus, M. Bykhovskaia, D. Woolard, B. Gelmont, *J. Phys. D* **2003**, *36*, 1314.
[98] M. Brucherseifer, M. Nagel, P. H. Bolivar, H. Kurz, *Appl. Phys. Lett.* **2000**, *77*, 4049.
[99] M. Nagel, F. Richter, P. H. Bolivar, H. Kurz, *Phys. Med. Biol.* **2003**, *48*, 3625.
[100] T. Globus, R. Parthasarathy, T. Khromova, D. Woolard, N. Swami, A. J. Gatesman, J. Waldman, *Proc. SPIE-Int. Soc. Opt. Eng.* **2004**, *5584*.
[101] R. Parthasarathy, T. Globus, T. Khromova, N. Swami, D. L. Woolard, *Appl. Phys. Lett.* **2005**, *87*, 113901.
[102] T. Globus, D. L. Wollard, T. W. Crowe, T. Khromova, B. Gelmont, J. Hesler, *J. Phys. D* **2006**, *39*, 3405.
[103] A. G. Markelz, A. Roitberg, E. J. Heilweil, *Chem. Phys. Lett.* **2000**, *320*, 42.
[104] M. Walther, B. Fischer, M. Schall, H. Helm, P. U. Jepsen, *Chem. Phys. Lett.* **2000**, *332*, 389.
[105] A. Markelz, S. Whitmire, J. Hillebrecht, R. Birge, *Phys. Med. Biol.* **2002**, *47*, 3797.
[106] S. E. Whitmire, D. Wolpert, A. G. Markelz, J. R. Hillebrecht, J. Galan, R. R. Birge, *Biophys. J.* **2003**, *85*, 1269.
[107] J.-Y. Chen, J. R. Knab, J. Cerne, A. Markelz, *Phys. Rev. E* **2005**, *72*, 040901R.
[108] J. Knab, J.-Y. Chen, A. Markelz, *Biophys. J.* **2006**, *90*, 2576.

[109] U. Heugen, G. Schwaab, E. Bründermann, M. Heyden, X. Yu, D. M. Leitner, M. Havenith, *Proc. Natl. Acad. Sci. USA* **2006**, *103*, 12301.
[110] E. Bründermann, D. R. Chamberlin, E. E. Haller, *Appl. Phys. Lett.* **1998**, *73*, 2757.
[111] C. Zhang, S. M. Durbin, *J. Phys. Chem. B* **2006**, *110*, 23607.
[112] C. Zhang, E. Tarhan, A. K. Ramdas, A. M. Weiner, S. M. Durbin, *J. Phys. Chem. B* **2004**, *108*, 10077.
[113] S. Bone, R. Pethig, *J. Mol. Biol.* **1982**, *157*, 157; S. Bone, R. Pethig, *J. Mol. Biol.* **1985**, *181*, 323.
[114] J. Xu, K. Plaxco, S. J. Allen, *Protein Sci.* **2006**, *15* 1175.
[115] J. Xu, K. Plaxco, S. J. Allen, *J. Phys. Chem. B* **2006**, *110*, 24255.
[116] H. W. T. van Vlijmen, M. Karplus, *J. Phys. Chem. B* **1999**, *103*, 3009.
[117] B. C. Dian, A. Longarte, S. Mercier, D. A. Evans, D. J. Wales, T. S. Zwier, *J. Chem. Phys.* **2002**, *117*, 10688.
[118] W. Chin, F. Piuzzi, I. Dimicoli, M. Mons, *Phys. Chem. Chem. Phys.* **2006**, *8*, 1033.
[119] D. Reha, H. Valdes, J. Vondrasek, P. Hobza, A. Abu-Riziq, B. Crews, M. S. de Vries, *Chem. Eur. J.* **2005**, *11*, 6803.
[120] M. Gerhards, C. Unterberg, A. Gerlack, A. Jansen, *Phys. Chem. Chem. Phys.* **2004**, *6*, 2682.
[121] A. Abo-Riziq, L. Grace, E. Nir, M. Kabelac, P. Hobza, M. S. de Vries, *Proc. Natl. Acad. Sci. USA* **2005**, *102*, 20.

Received: May 10, 2007
Published online on November 7, 2007

